©2006 Society of Economic Geologists, Inc.
Economic Geology, v. 101, pp. 281–310

Geology, Geochronology, and Hf and Pb Isotope Data of the Raúl-Condestable Iron Oxide-Copper-Gold Deposit, Central Coast of Peru

Antoine de Haller,[†,*]

University of Geneva, Mineralogy Department, rue des Maraîchers 13, CH-1205 Genève, Switzerland

Fernando Corfu,

University of Oslo, Department of Geosciences, Postbox 1047 Blindern N-0316 Oslo, Norway

Lluís Fontboté, Urs Schaltegger,

University of Geneva, Mineralogy Department, rue des Maraîchers 13, CH-1205 Genève, Switzerland

Fernando Barra,

Department of Geociences, University of Arizona, Tucson, Arizona 85721, and Instituto de Geología Económica Aplicada, Universidad de Concepción, Concepción, Chile

Massimo Chiaradia,

University of Geneva, Mineralogy Department, rue des Maraîchers 13, CH-1205 Genève, Switzerland

Martin Frank,[**]

Institute for Isotope Geology and Mineral Resources, Department of Earth Sciences, ETHZ, NO F51.3, Sonneggstrasse 5, CH-8092 Zürich, Switzerland

and Julio Zúñiga Alvarado

Cía. Minera Condestable S.A., Calle Manuel Roaud y Paz Soldán 364, San Isidro, Lima 27, Peru

Abstract

Raúl-Condestable is a >32 million metric ton (Mt) iron oxide-copper-gold (IOCG) deposit located on the Peruvian coast, 90 km south of Lima. The ore occurs as veins, replacement "mantos," and disseminations consisting of a chalcopyrite-pyrite-pyrrhotite-magnetite-amphibole mineral association. The geology of the studied area comprises a series of superposed volcanic edifices of Late Jurassic to Early Cretaceous age, which are part of a larger volcanic island to continental arc system. Particularly good exposures of the tilted host sequence allow the mapping of the Raúl-Condestable IOCG deposit in a nearly complete oblique cross section, from its associated volcanic edifice down to a paleodepth of about 6 km.

U-Pb zircon ages indicate that in the deposit area felsic magmatic activity took place between 116.7 ± 0.4 and 114.5 ± 1 Ma, defining a new Raúl-Condestable superunit, the oldest so far, of the Peruvian Coastal batholith. This superunit is located west of the main part of the batholith and includes a dacite-andesite volcanic dome and a subvolcanic quartz-diorite porphyry sill-dike complex that were emplaced at 116.7 ± 0.4 and 116.4 ±0.3 Ma, respectively, followed by tonalite stocks and dikes emplaced between 115.1 ± 0.4 and 114.5 ± 1 Ma. All these rocks contain hornblende and/or biotite but no pyroxene and correspond to silica- and water-rich magmas following a calcic differentiation trend. Hf isotope data on zircons (ε_{Hf}(115 Ma) = 5.2–7.5) and Pb isotope data on whole rock, combined with lithogeochemical results, suggest that magmas were generated by partial melting of the upper mantle, enriched through hydrous metasomatism and/or melting of subducted pelagic sediments. The lack of zircon inheritance suggests that there was no direct involvement of continental crust.

The Raúl-Condestable IOCG deposit is connected in space and time with the magmatism of the Raúl-Condestable superunit. The mineralization was emplaced in the core of the dacite-andesite volcanic dome at a paleodepth of 2 to 3 km, surrounding two tonalitic intrusions formed at 115.1 ± 0.4 and 114.8 ± 0.4 Ma. The U-Pb age of hydrothermal titanite from IOCG veins at 115.2 ± 0.3 Ma indicates that the mineralization was coeval with (or more probably just followed) the emplacement of the tonalites. Re-Os geochronology on molybdenite did not yield reliable ages due to apparent Re loss. Copper ore is associated with a zoned alteration pattern, which surrounds the tonalite intrusions. It consists of a core of biotite alteration and quartz stockwork,

[†] Corresponding author: email, antoine.dehaller@terre.unige.ch

[*] The digital Appendix is available at <http://segweb.org/EG/papers/Abs 101-2_files/deHallerAppendix.pdf>.

[**] Present address: IfM-GEOMAR, Leibniz Institute for Marine Sciences at the University of Kiel, Wischhofstrasse 1-3, 24148 Kiel, Germany.

0361-0128/06/3576/281-30 $6.00

grading outward to actinolite (±magnetite, ±chlorite, ±titanite, ±scapolite, ±albite, ±epidote) and upward to sericite + Fe chlorite alteration. An upper distal alteration halo consisting of hematite-chlorite surrounds the sericite + Fe chlorite and actinolite alterations laterally. Most of the ore is spatially associated with the actinolite alteration and, to a lesser extent, with the sericite + Fe chlorite alteration.

The results of this study confirm that the 110 to 120 Ma age range was a productive time period for Andean IOCG deposits. The characterization of the hydrous intermediate magmatism related to the mineralization, as well as the subvolcanic position of the deposit and its related alteration pattern provides further criteria that may be used when exploring for IOCG deposits in a convergent plate tectonic setting.

Introduction

The Raúl-Condestable deposit, with estimated combined reserves plus production of >32 million metric tons (Mt) at 1.7 percent Cu, 0.3 g/t Au, and 6 g/t Ag is located approximately 90 km south of Lima on the Peruvian coast (Fig. 1). Associations of chalcopyrite-pyrite-pyrrhotite-magnetite-amphibole occur as veins, replacement "mantos," and disseminations in a Late Jurassic to Early Cretaceous volcano-sedimentary sequence cut by felsic to mafic intrusions. Studies by various authors of the Raúl-Condestable deposit have led to contrasting interpretations. Ripley and Ohmoto (1977, 1979), Wauschkuhn (1979), and Cardozo (1983) proposed a volcanic-exhalative genesis, whereas Injoque (1985), Atkin et al. (1985), and Vidal et al. (1990) favored a skarn-type mineralization. Recently, de Haller (2000, 2006), de Haller et al. (2001, 2002), Injoque (2002), Sillitoe (2003), and Williams et al. (2005) have considered Raúl-Condestable to be an iron oxide-copper-gold (IOCG) deposit.

Although arc plutonism has been shown to be coeval with mineralization for many Andean IOCG deposits (Sillitoe, 2003, and references therein; Williams et al., 2005), there are still major uncertainties regarding the type of associated magmas, their source, their depth of emplacement, their spatial relationship with ore and alteration, and the nature of the underlying basement.

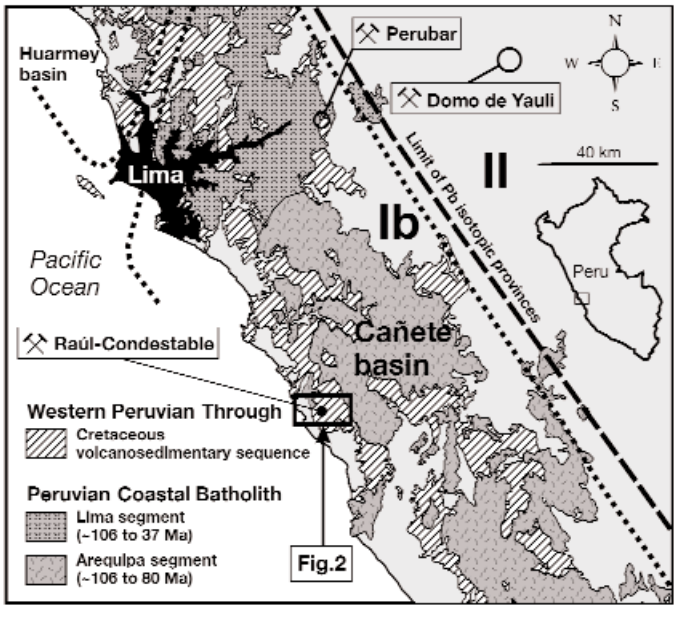

Fig. 1. Location and regional geologic setting of the Raúl-Condestable iron oxide-copper-gold deposit in the central coast of Peru. The location of the studied area (Fig. 2) is shown. Ages are from Mukasa and Tilton (1985a) and Mukasa (1986a). Pb isotope provinces Ib and II are from MacFarlane et al. (1990). Boundaries of the Huarmey and Cañete Cretaceous basins are from Cobbing (1978). Each segment of the Peruvian Coastal batholith is composed of various "superunits" or magmatic suites (e.g., Atherton and Sanderson, 1985; Pitcher, 1985). In the studied area, the Patap superunit crops out on the western flank of the batholith.

This paper investigates the possible temporal relationships between the Raúl-Condestable IOCG mineralization and the magmatic rocks of the area, the geologic and geotectonic context of the ore deposit, its alteration halo, and the possible sources and characteristics of the associated magmatism. The particularly good exposure of the tilted host sequence allows the mapping of the Raúl-Condestable IOCG deposit in a nearly complete oblique cross section, from its associated volcanic edifice down to a paleodepth of about 6 km.

The time-constrained geologic model we propose is supported by new geologic maps and sections, whole-rock geochemical data, U-Pb dating of hydrothermal titanite from IOCG veins as well as of zircon from magmatic rocks, IOCG molybdenite Re-Os isotope data, zircon Hf isotope data, and Pb isotope data on sulfides and whole rocks. The conclusions of this study have implications for IOCG exploration in volcanic arc settings and for the understanding of the geology of the central coast of Peru. A detailed study of the alteration, geochemistry, sulfur isotopes, and fluid chemistry of the ore-forming system will be presented in another paper, derived from de Haller (2006).

Geologic Context

The studied area forms part of the western Peruvian trough (Wilson, 1963; Cobbing, 1985; Jaillard et al., 1990), which is a mostly Cretaceous volcano-sedimentary belt that crops out along the central coast of Peru (Fig. 1). Cobbing (1978) divided the western Peruvian trough into five basins, with the studied area being located in the northern part of the Cañete basin, near the southern limit of the Huarmey basin (Fig. 1). This volcano-sedimentary sequence includes basaltic to rhyolitic lava, pyroclastic deposits, tuff, limestone, shale, sandstone, and locally, evaporite. The geology of the western Peruvian trough is complex, with strong lateral facies changes, and the literature dedicated to this sequence is fragmented and frequently contradictory (Wilson, 1963; Rivera et al., 1975; Guevara, 1980; Osterman et al., 1983; Atherton et al., 1985; Jaillard et al., 1990; Palacios et al., 1992; Salazar and Landa, 1993; Vela, 1997; Benavides-Cáceres, 1999). Many problems remain concerning the nomenclature of lithostratigraphic units (Vela, 1997) and their respective ages, which are essentially based on scarce macropaleontological data (mostly Rivera et al., 1975; Palacios et al., 1992; Salazar and Landa, 1993; and references therein) thought to correspond to the late Tithonian to Cenomanian interval (~147–93.5 Ma: Gradstein et al., 1995). Apart from the U-Pb zircon ages presented in this paper, few absolute ages are available for the western

Peruvian trough, all falling within the Late Cretaceous to Paleocene interval (U-Pb ages in Polliand et al., 2005; $^{40}Ar/^{39}Ar$ ages in Noble et al., in press, a and b).

Farther inland, the western Peruvian trough is intruded by the Peruvian Coastal batholith (Fig. 1), which has an outcrop length of 1,600 km and is up to 65 km wide (Pitcher et al., 1985; Mukasa, 1986a; Haederle and Atherton, 2002). The Coastal catholith consists of a series of telescoped tabular intrusions that were emplaced at high crustal level through a combination of roof-lifting and cauldron subsidence (Pitcher et al., 1985). It is made up of composite and multiple calc-alkaline to tholeiitic intrusions, dominantly composed of tonalite and granodiorite and subdivided into units and superunits (Pitcher, 1985). The units have been defined as chemically and mineralogically homogeneous and coetaneous magmatic pulses, whereas superunits consist of groups of units with close spatial and temporal association, corresponding to consanguineous rock suites (Atherton and Sanderson, 1985). Although this "unit" and "superunit" nomenclature is not recognized by the American Geological Institute, it is used in this paper for purpose of consistency with previous works on the Peruvian Coastal batholith (including the geologic map of Peru by the Instituto Geológico Minero y Metalúrgico). Age relationships between the superunits show an eastward migration of the magmatic activity with time (Pitcher, 1985; Mukasa, 1986a). Based on the superunit assemblages, three main segments were defined along the batholith belt. From north to south, the Lima segment has ages from ~106 to 37 Ma, the Arequipa segment from ~106 to 80 Ma, and the Toquepala segment from about 190 to 57 Ma (Beckinsale et al., 1985; Moore and Agar, 1985; Mukasa and Tilton, 1985a; Pitcher, 1985; Mukasa, 1986a). The studied area is located within the northern part of the Arequipa segment, close to the boundary with the Lima segment (Fig. 1). Common to these two segments, the Patap superunit (comprising early basic intrusions: Regan, 1985) is the oldest superunit described in the batholith. The existing U-Pb data on zircon and K-Ar data on hornblende and plagioclase [zircon = 84 ± 0.4 Ma, hornblende = 75 ± 3 (2σ) Ma, plagioclase = 92 ± 2 (2σ) Ma] for the Patap superunit are problematic from a geologic point of view (Beckinsale et al., 1985; Mukasa and Tilton, 1985a) as crosscutting relationships favor a 106 to 101.4 Ma age (Mukasa, 1986a). We will demonstrate further that plutonic activity on the western flank of the Peruvian Coastal batholith is older than the Patap superunit itself.

The geochemistry of both the western Peruvian trough volcanic rocks and the Peruvian Coastal batholith falls mainly in the calc-alkaline field, but a tholeiitic affinity is recorded for the Patap superunit and the Casma Group (western Peruvian trough: Albian to Cenomanian age) north of Lima (Regan, 1985; Atherton and Webb, 1989). Strontium (Beckinsale et al., 1985), Pb (Mukasa and Tilton, 1985b; Mukasa, 1986b; Macfarlane et al., 1990), and Hf (Polliand et al., 2005) isotope data suggest the absence of cratonic basement in the Lima segment up to Trujillo and in the Arequipa segment down to Chimbote. By contrast, varying degrees of interaction with Precambrian basement (Arequipa Massif: Cobbing, 1985; Wasteneys et al., 1995) are indicated by Sr and Pb isotope data in the southern part of the Arequipa segment and in the Toquepala segment. These findings are in agreement with geophysical data showing the presence of a high-density (3 g/cm^3) structure within the upper crust below the western Peruvian trough in central Peru from Pisco to Trujillo, thus precluding the presence of a sialic basement in this area (Couch et al., 1981; Jones, 1981; Wilson, 1985). These facts have led to a debate on the tectonic setting of both the western Peruvian trough and the Peruvian Coastal batholith, with two main theories being proposed.

Atherton et al. (1985), Aguirre et al. (1989), Atherton and Webb (1989), Atherton and Aguirre (1992), and Cobbing (1998) favor an aborted back-arc setting. They explain the tholeiitic affinity of some of the rocks and the existence of the dense structure below the western Peruvian trough as evidence of mantle doming, coeval with crustal thinning, subsidence, and the western Peruvian trough volcanism. In this model, some authors suggest that the Early Cretaceous volcanic arc itself is located to the west of the present coastline, on the so-called Outer Shelf High or Paracas Block (Myers, 1974, Benavides-Cáceres, 1999) or Coastal Cordillera (Guevara, 1980), whereas others suggest a lack of subduction at that time and the absence of an active volcanic arc (Atherton and Webb, 1989).

By contrast, Soler (1991a, b) suggests a volcanic arc setting for the western Peruvian trough, which was active under oblique subduction and underwent local intra-arc extension via a pull-apart mechanism. Recently, Haeberlin et al. (2004) proposed an alternative explanation for the lack of sialic cratonic material below the western Peruvian trough: the high-density basement is thought to correspond to a piece of oceanic crust that formed during the Paleozoic through the removal and northward migration of the northern part of the Arequipa Massif. Polliand et al. (2005) present interpretations based on U-Pb, Hf, and geologic data from the eastern part of the western Peruvian trough at the latitude of Lima that are in agreement with the intra-arc extensional (pull-apart) model of Soler (1991b) and support the lack of sialic basement underlying this part of the Peruvian coast.

The field, geochemical, and isotopic data from the Raúl-Condestable deposit area presented in this study are in close agreement with this second model.

Methodology

Geologic mapping and interpretation

The geologic map presented in this paper is the result of fieldwork on a >50-km^2 area undertaken by the senior author for the Cía. Minera Condestable S.A (Figs. 2, 3). Field data were complemented with information from previously published geologic maps of the Raúl-Condestable deposit area (Cardozo, 1983; Atkin et al., 1985; Injoque, 1985; Salazar and Landa, 1993), as well as unpublished reports for Cía. Minera Condestable S.A. by J. Zúñiga (1998) and for Cía. Minera Pativilca S.A. by R. Flores (1992). Detailed mapping at a 1:2,000 scale was undertaken in the deposit area, where the geologic map of the Cía. Minera Condestable S.A. property was extended to the neighboring Raúl mine area on the basis of a 1:2,000 topographic map drawn by Cía. Minera Condestable S.A (Fig. 2). A larger area surrounding the deposit was mapped at 1:25,000. Thin section microscopy and whole-rock X-ray diffraction were used for the determination of the

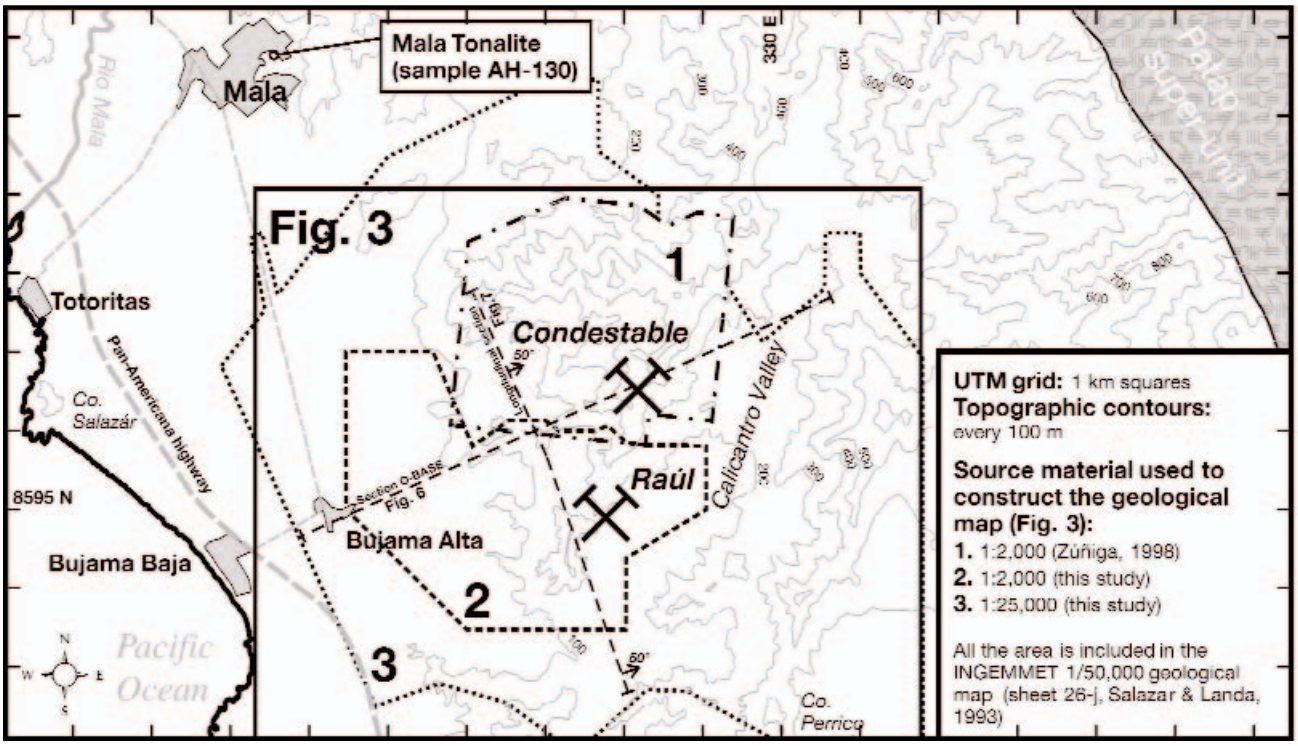

FIG. 2. Topographic map of the studied area. The position and scale of the survey areas used to construct the geologic map of Figure 3 are shown. Sections 0-BASE and longitudinal are shown in Figures 6 and 7, respectively. The Patap superunit shown in the northeastern corner of the map is part of the Peruvian Coastal batholith (see text). Topography is from a 1:25,000 map of the Ministry of Agriculture of Peru. The main source material for area 1 is an unpublished report for Cía. Minera Condestable S.A. by J. Zúñiga (1998).

alteration mineral assemblages shown in Figures 3 and 4 and in Table 1.

The lithostratigraphic column presented in Figure 5 is based on the information collected during the geologic mapping, correlated with information from the literature (Rivera et al., 1975; Palacios et al., 1992; Salazar and Landa, 1993). The detailed lithostratigraphic column of the unit hosting the mineralization (unit III) shown in Figure 5 is mostly based on unpublished information collected by the staff of both Raúl and Condestable mining operations (R. Flores, 1992, and J. Zúñiga, 1998, unpub. reports for Cía. Minera Pativilca S.A. and Cía. Minera Condestable S.A.).

Based on surface, underground, and drill data, a constant dip of 40° to the west-southwest is evident in both the Condestable and Raúl mines. Including Figure 6, 26 transverse sections were drawn, which served as a base for the drawing of the longitudinal section shown in Figure 7. The locations of the transverse and longitudinal sections are shown in Figures 2, 3, and 4. Information from mine (both Raúl and Condestable) geologic sections and maps (1:500 scale) was used as a base for the drawing of the sections in the operating areas.

Pb isotopes

Sulfides were prepared following the method described in Chiaradia et al. (2004). For whole rock, about 100 mg of powdered sample was digested in cap-sealed Teflon vials with a mixture of 1 ml 14*M* HNO_3 and 4 ml 29*M* HF for 7 d, and lead was purified by extraction chromatography using an Sr-Spec resin.

Purified lead fractions of sulfides and whole rocks were loaded onto Re filaments with the silica gel technique and

FIG. 3. Geologic map of the Raúl-Condestable deposit area. For readability, only the main dolerite dikes are shown. Sections 0-BASE and longitudinal are shown respectively in Figures 6 and 7. Limits of outcrops and covered areas are based on field data and interpretation of a panchromatic SPOT satellite image (10-m pixels). The geologic interpretation of areas covered by recent deposits is based on underground and drill data in the operation area and locally by drill data away from the mining center. The whole volcano-sedimentary sequence is tilted about 40° to the west-southwest, so that the geologic map broadly corresponds to an oblique cross section through the deposit, from its associated volcanic edifice (unit IV) down to a paleodepth of about 6 km. The Condestable fault is a major structure intruded by a quartz-diorite porphyry dike, with an apparent normal movement of about 500 m. The transitional boundary between alteration mineral assemblages is represented schematically by a zigzag pattern. Biotite and quartz stockwork alterations surround tonalitic intrusions and grade laterally to actinolite alteration. A sericite-Fe chlorite alteration is present on top of the system, mainly in unit IV, and grades laterally to hematite-chlorite alteration. Copper ore is mostly found associated with actinolite alteration.

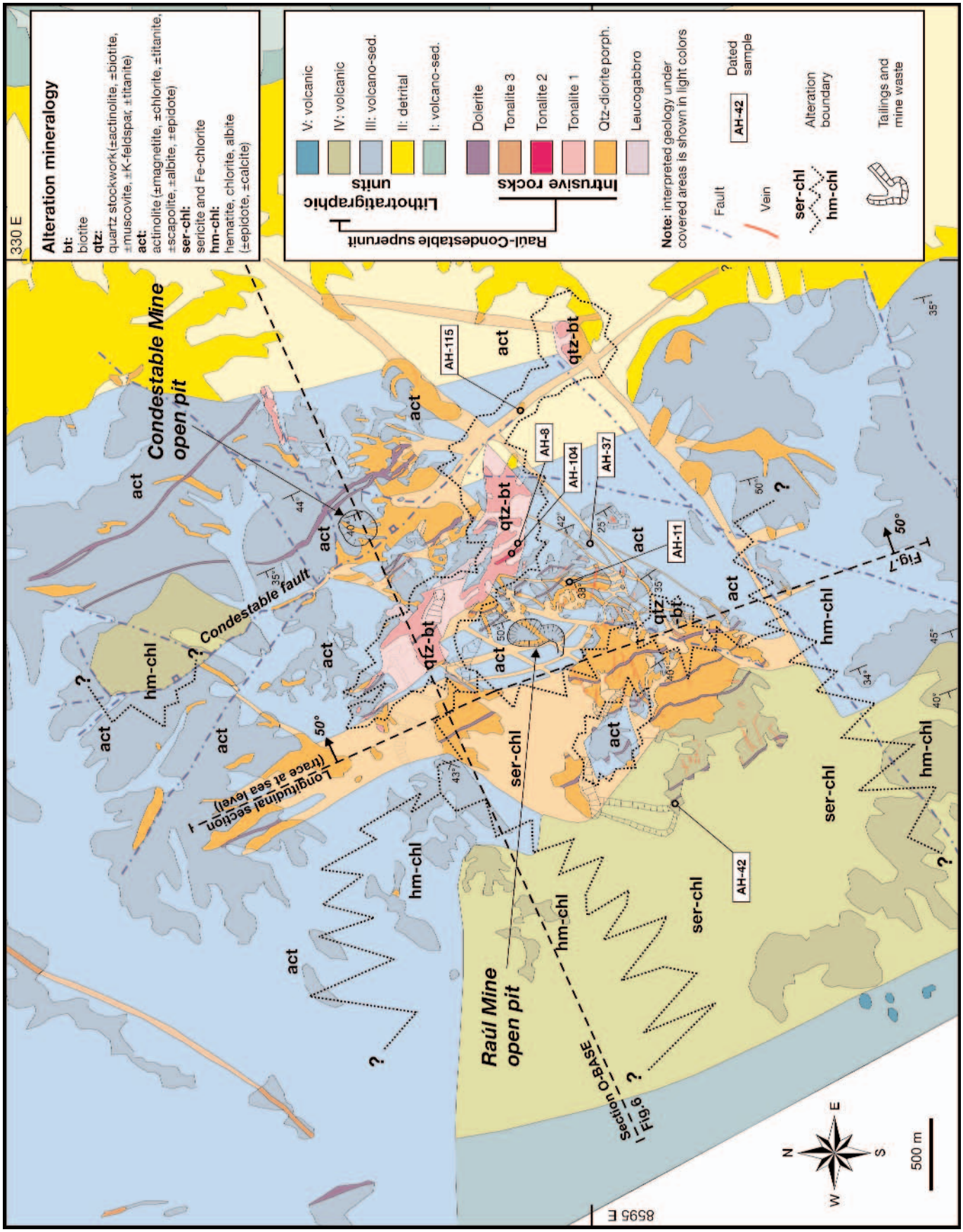
Alteration mineralogy
bt:
biotite
qtz:
quartz stockwork (±actinolite, ±biotite, ±muscovite, ±K-feldspar, ±titanite)
act:
actinolite (±magnetite, ±chlorite, ±titanite, ±scapolite, ±albite, ±epidote)
ser-chl:
sericite and Fe-chlorite
hm-chl:
hematite, chlorite, albite (±epidote, ±calcite)
Raúl-Condestable supergroup
Lithostratigraphic units
V: volcanic
IV: volcanic
III: volcano-sed.
II: detrital
I: volcano-sed.
Intrusive rocks
Dolerite
Tonalite 3
Tonalite 2
Tonalite 1
Qtz-diorite porph.
Leucogabbro
Note: interpreted geology under covered areas is shown in light colors
Fault
Vein
Dated sample
AH-42
Alteration boundary
ser-chl
hm-chl
Tailings and mine waste
8330 E
8595 E
Condestable Mine open pit
Raúl Mine open pit
Condestable fault
Longitudinal section (trace at sea level)
Section O-BASE
Fig. 6
Fig. 7
act
qtz-bt
ser-chl
hm-chl
AH-115
AH-8
AH-104
AH-37
AH-11
AH-42
N
S
E
W
500 m

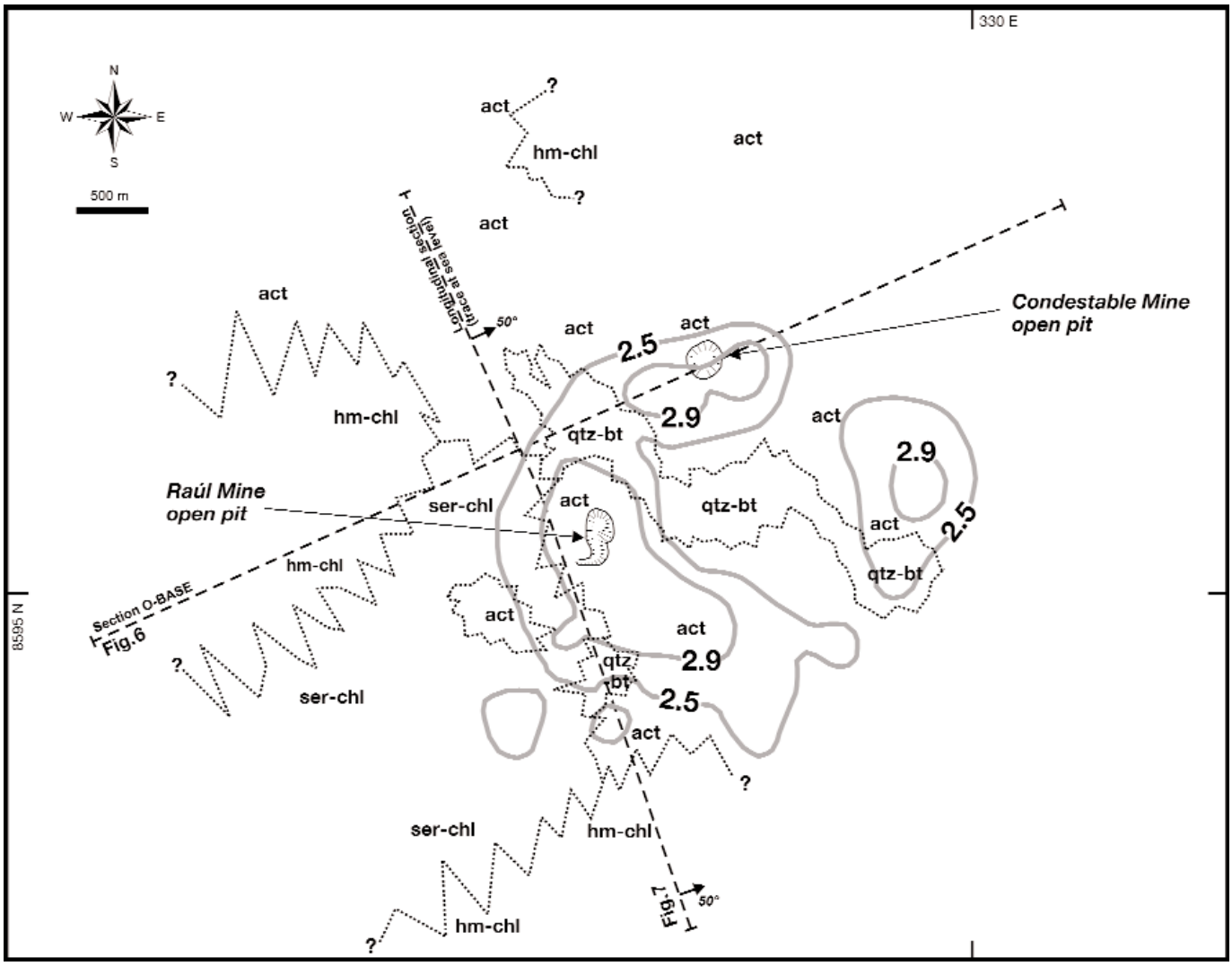

FIG. 4. Relationship between the alteration assemblages and the copper anomaly. Same legend as Figure 3. The log parts per million copper geochemical contours were obtained through the kriging of 238 ICP analyses from 204 surface rock chip samples and 34 composite samples from surface drilling. Log values 2.5 and 2.9 correspond to about 315 and 796 ppm Cu, respectively.

isotope ratios were measured on an MAT-262 mass spectrometer at the Department of Mineralogy, University of Geneva, Switzerland. Lead isotope ratios were corrected for fractionation by a +0.08 percent amu factor based on more than 100 analyses of the SRM981 standard. The analytical uncertainties (2σ) were 0.05 percent for $^{206}Pb/^{204}Pb$, 0.08 percent for $^{207}Pb/^{204}Pb$, and 0.10 percent for $^{208}Pb/^{204}Pb$. Procedural blanks were always <120 pg Pb so that no blank correction on the results was required.

U-Pb isotopes

Samples weighing 0.3 to 1 kg were crushed and milled with a disc mill. Zircon and titanite were concentrated on a Wilfley table, by Frantz magnetic separator, and bromoform heavy liquid. Dated zircon and titanite fractions were homogeneous in terms of color and morphology, and grains were free of cracks and inclusions unless otherwise indicated. For each sample, repeated analyses were performed to increase the age precision and detect possible lead loss or inheritance.

Zircon and titanite analyses were carried out by isotope dilution at the University of Oslo. Details of the procedure and parameters used are given in Corfu (2004). The only differences were the chemical separation of titanite by a single-stage HBr-HCl-HNO_3 procedure (Corfu and Andersen, 2002). The initial common Pb in zircon was corrected using the Pb isotope composition predicted by the model of Stacey and Kramers (1975) for the age of the sample and propagating conservative uncertainties of ±1 percent for the 207/204 and ± 2 percent for the 206/204 ratio. The initial common Pb in hydrothermal titanite was corrected using the average composition of five pyrite samples from the same main hydrothermal stage as titanite: 206/204 = 18.606 (±0.05%), 207/204 = 15.652 (±0.08%), and 208/204 = 38.577 (±0.1%). Data plotting and age calculations were performed with the program ISOPLOT of Ludwig (1999).

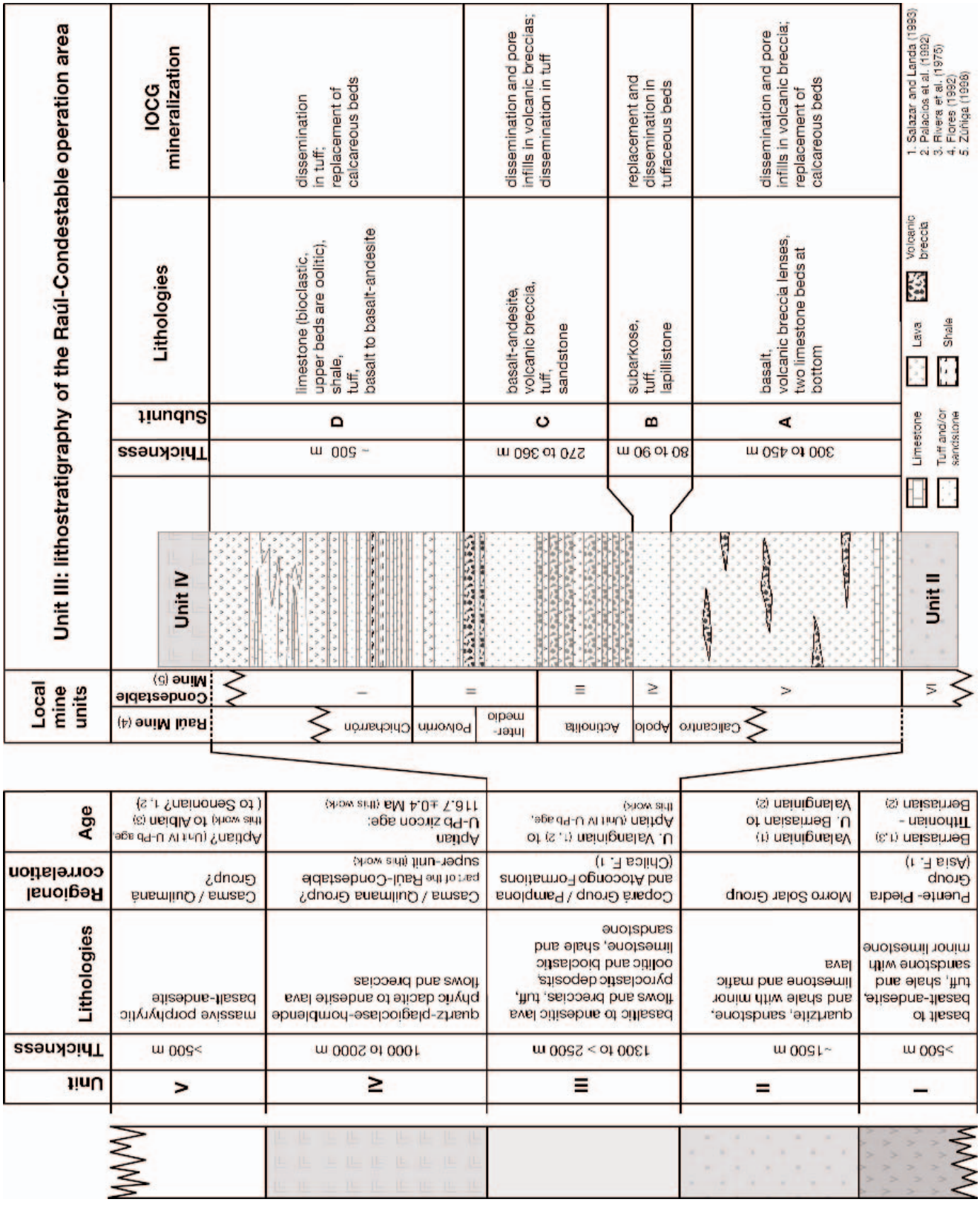

FIG. 5. Lithostratigraphic column of the Raúl-Condestable area. A detailed description of each unit and subunit is given in the text. References 4 and 5 correspond to two unpublished reports, by R. Flores (1992) for Cía. Minera Pativilca S.A., and by J. Zúñiga (1998) for Cía. Minera Condestable S.A, respectively.

TABLE 1. Representative Whole-Rock XRF Analyses of Igneous Rocks from the Raúl-Condestable Deposit Area

		Raúl-Condestable superunit									Patap superunit
Rock		Unit IV dacite	Quartz-diorite porphyry		Tonalite 1		Tonalite 2	Tonalite 3		Mala Tonalite	Gabbro
Sample number		AH-42	AH-72	AH-115	AH-8	AH-111	AH-104	AH-120	AH-121	AH-130	AH-2C
Long. (UTM)		326234	327470	328950	328045	328460	327975	325100	325100	323575	334583
Lat. (UTM)		8594423	8594920	8595500	8595509	8595620	8595550	8598850	8598850	8600825	8597732
Alteration minerals[1]		chl+ser (+cal)	act+chl (+ser)	act+chl (+ser)	chl+act+ep+ser	(chl+ser+cal+ep)	(chl+ep+cal)	(chl+ser+ep)	(act+chl+ser)	(chl+ser+ep)	act+czo+chl
Major elements (%)	SiO_2	64.67	64.28	65.78	60.68	67.46	65.53	65.89	55.60	61.90	47.00
	TiO_2	0.41	0.47	0.40	0.55	0.39	0.41	0.50	0.80	0.52	0.47
	Al_2O_3	16.32	17.47	17.06	17.69	16.23	16.25	15.93	16.54	17.56	20.22
	Fe_2O_3	7.16	3.93	3.89	5.62	2.52	4.34	3.76	9.42	5.43	9.21
	MnO	0.21	0.04	0.06	0.07	0.19	0.18	0.05	0.26	0.11	0.16
	MgO	1.79	1.79	1.26	2.18	1.53	1.56	2.14	3.73	1.89	6.25
	CaO	1.20	6.02	5.42	4.69	4.29	3.57	4.47	7.51	5.79	13.69
	Na_2O	2.23	4.82	4.43	4.57	4.61	4.29	4.16	2.87	3.85	1.47
	K_2O	3.13	0.52	0.33	1.12	0.70	1.35	1.15	0.98	1.24	0.37
	P_2O_5	0.16	0.18	0.18	0.20	0.15	0.16	0.12	0.20	0.19	0.04
	Cr_2O_3	0.02	0.04	<0.01	<0.01	<0.01	<0.01	0.01	0.01	<0.01	0.03
	NiO	<0.01	<0.01	<0.01	<0.01	<0.01	<0.01	<0.01	<0.01	<0.01	<0.01
	LOI	2.82	0.92	0.69	1.72	1.13	1.40	1.02	1.19	0.76	1.05
	Total	100.10	100.47	99.50	99.08	99.20	99.03	99.20	99.10	99.23	99.96
Trace elements (ppm)	Nb	6	6	5	7	7	9	7	4	7	1
	Zr	111	109	113	111	123	100	83	124	108	32
	Y	14	18	9	17	16	21	17	24	19	11
	Sr	105	332	394	327	307	268	345	412	358	327
	U	<2	<2	<2	<2	<2	2	<2	4	2	<2
	Rb	77	16	9	37	18	28	33	28	35	15
	Th	4	2	4	4	2	8	3	6	3	<2
	Pb	26	9	10	8	6	8	7	15	8	12
	Ga	19	18	19	19	17	19	17	17	18	16
	Zn	893	45	56	46	42	69	28	89	58	52
	Cu	18	475	337	4	4	20	5	34	2	36
	Ni	6	9	<2	<2	2	<2	7	10	4	12
	Cr	76	206	16	9	15	11	26	24	12	153
	V	28	26	38	38	7	34	66	219	55	255
	Ce	25	27	14	17	22	35	16	18	16	12
	Nd	10	12	6	8	11	16	8	12	10	5
	Ba	886	154	167	320	381	770	500	553	337	166
	La	6	9	8	9	12	18	9	9	8	<4
	S	<3	333	48	<3	<3	<3	<3	<3	<3	4
	Sc	<2	12	11	13	9	12	8	24	10	37
	As	4	<3	4	<3	5	3	<3	<3	<3	5

TABLE 1 *(Cont.)*

			Subunit IIIA	Subunit IIIC		Subunit IIID					Unit V
Rock		Dolerite	lava	leucogabbro	lava	lava				tuff	lava
Sample number		AH-7	AH-58	AH-75	AH-59	AH-31	AH-52	AH-67	AH-60	AH-76	AH 138
Long. (UTM)		327440	328487	327612	327874	327012	324942	326569	327754	328110	324900
Lat. (UTM)		8594278	8595324	8596386	8595085	8597988	8596877	8597859	8594659	8596600	8593079
Alteration minerals[1]		chl+ep+ser	bt+act (+chl)	ser+chl	act (+chl+cal)	ep+chl+cal	chl+mt+ser+ep +cal (+hem)	preh+chl+act +cal+ep	act+chl	chl+ser+sulfide	chl+ser+cal
Major elements (%)	SiO_2	49.93	50.92	50.10	51.47	53.60	52.27	50.86	51.09	55.53	52.38
	TiO_2	1.32	1.04	0.91	0.88	0.84	1.65	1.44	0.96	1.01	1.22
	Al_2O_3	15.42	18.71	22.24	16.42	18.16	16.12	16.75	16.45	20.34	16.95
	Fe_2O_3	12.82	10.58	3.72	7.33	6.63	10.02	8.23	10.05	5.88	10.35
	MnO	0.27	0.13	0.06	0.18	0.13	0.12	0.11	0.08	0.02	0.53
	MgO	4.34	4.59	4.43	6.32	6.29	3.30	5.50	6.01	2.37	3.46
	CaO	8.55	8.09	10.93	10.21	3.20	5.45	8.09	10.05	1.96	3.58
	Na_2O	3.31	4.05	4.01	3.71	7.19	6.40	5.24	3.35	7.26	3.98
	K_2O	1.15	0.96	0.77	0.78	0.12	0.38	0.32	0.31	1.68	2.67
	P_2O_5	0.21	0.19	0.13	0.24	0.19	0.42	0.31	0.17	0.12	0.25
	Cr_2O_3	0.01	0.01	0.02	0.07	0.03	0.01	0.04	0.03	0.03	<0.01
	NiO	<0.01	<0.01	<0.01	0.01	0.01	<0.01	0.01	<0.01	0.01	<0.01
	LOI	1.84	1.06	2.31	2.33	3.79	4.13	3.02	0.74	3.83	3.53
	Total	99.16	100.32	99.64	99.94	100.17	100.28	99.92	99.30	100.03	98.91
Trace elements (ppm)	Nb	4	2	2	8	11	14	15	6	24	8
	Zr	97	60	60	119	111	271	165	96	160	182
	Y	25	21	18	29	22	36	26	22	40	33
	Sr	377	296	484	248	175	172	304	153	337	181
	U	2	<2	<2	2	2	3	2	<2	4	3
	Rb	26	29	30	26	4	12	9	9	72	64
	Th	5	<2	<2	3	4	10	4	4	16	8
	Pb	15	7	4	17	<2	2	4	10	5	5
	Ga	20	23	18	19	17	22	22	18	28	18
	Zn	163	87	63	96	93	74	92	60	46	157
	Cu	108	27	137	503	114	29	301	231	351	118
	Ni	11	15	10	49	76	16	59	21	50	9
	Cr	29	97	133	461	225	94	225	127	184	25
	V	389	375	227	186	125	379	275	255	187	300
	Ce	25	25	29	49	21	47	32	14	80	38
	Nd	14	11	14	28	<4	21	16	7	30	18
	Ba	496	203	176	338	68	86	106	41	236	1530
	La	15	9	16	10	6	10	6	9	32	17
	S	26	<3	129	16	<3	<3	426	<3	7169	6
	Sc	38	39	19	32	33	39	26	38	22	36
	As	7	4	<3	<3	5	6	6	<3	17	<3

[1]act = actinolite, bt = biotite, cal = calcite, chl = chlorite, czo = clinozoizite, ep = epidote, hm = hematite, mt = magnetite, preh = prehnite, ser = sericite

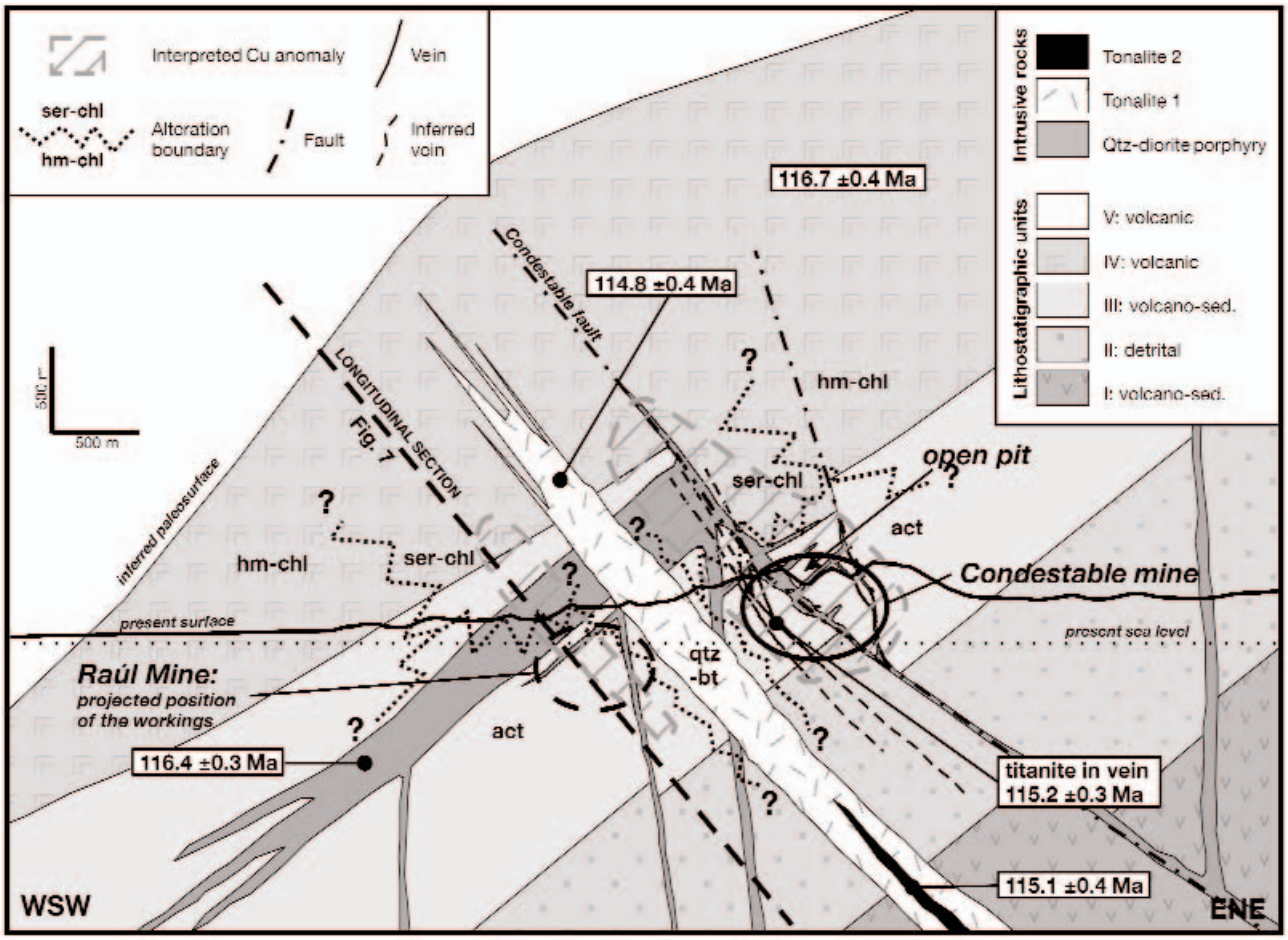

FIG. 6. Transverse section O-BASE. This section crosses the Condestable mine and shows the geologic framework of the deposit. Its location is shown in Figures 2, 3, and 4. The top of unit IV is thought to correspond to the paleosurface at the time of the mineralization. Therefore, the deposit is located in a subvolcanic position at a paleodepth of 2 to 3 km. Dolerite dikes cut the whole sequence including unit V and are not shown. The dip and offset of the Condestable fault quartz-diorite porphyry dike (Fig. 3) are well known from underground and drill data in the working area of the Condestable mine. Symbols of the alteration assemblages are explained in Figure 3. The tonalite 1 stock is surrounded by a biotite alteration halo, itself overprinted by a quartz stockwork. Biotite grades laterally to actinolite alteration, which is associated with most of the copper mineralization. The top of the system is dominated by a sericite + Fe chlorite assemblage. Hematite-chlorite alteration occurs in an upper lateral position. The longitudinal section is shown in Figure 7.

Hf isotopes

The Hf-Zr-REE fraction was collected during U-Pb column chemical separation. The Hf isotope analyses were carried out at the Federal Institute of Technology (ETH) in Zürich, Switzerland, following the same analytical method and using the same parameters as in Schaltegger et al. (2002). Errors of the measured $^{176}Hf/^{177}Hf$ ratios are given as external 2σ reproducibility of standard measurements for each individual session. Epsilon Hf values were calculated with $(^{176}Hf/^{177}Hf)_{CHUR(0)} = 0.282772$ (Blichert-Toft and Albarède, 1997) for an age of 115 Ma.

Re-Os isotopes

Rhenium-Os analyses were undertaken at the University of Arizona, Tucson, on two molybdenite samples from IOCG veins, following the method described in Barra et al. (2003). Molybdenite in both samples is medium grained (<2 mm) and was separated by handpicking. The five analyzed fractions were >50 mg to avoid possible Re-Os decoupling effects (e.g., Stein et al., 2001; Selby and Creaser, 2004). The 2σ error calculated by error propagation includes the uncertainties of the spike calibrations (0.08% for Re and 0.15% for Os), the decay constant error (0.31%), and analytical errors.

Local Geology: A Field-Based Revision

The extensive field work undertaken by the senior author in the Raúl-Condestable deposit area allows for a revision of the local geology, previously presented by Ripley and Ohmoto (1977, 1979), Cardozo (1983), Atkin et al. (1985), Injoque (1985), and Vidal et al. (1990).

The Raul-Condestable sequence (Fig. 3), a part of the western Peruvian trough, reaches a total thickness of more than 6 km, and dips to the west-southwest at an angle of around 40°. It is divided into five units (units I to V, from bottom to top: Fig. 5), with interpreted ages ranging from the Late Jurassic (beginning of Tithonian: 150.7 ± 3.0 Ma, Gradstein et al.,

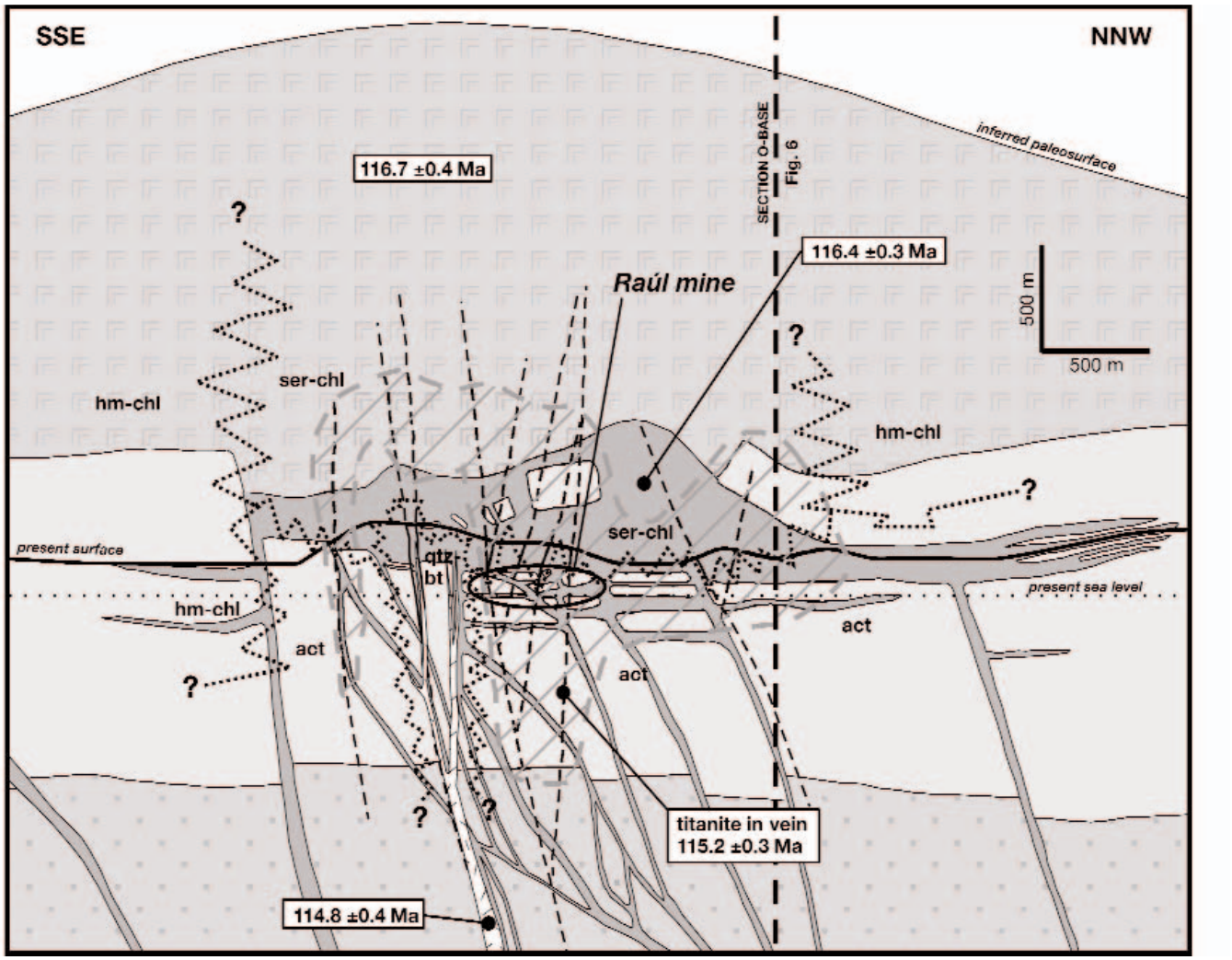

FIG. 7. Longitudinal section. This section is perpendicular to the bedding plane and dips 50° eastward (see Fig. 6). It crosses the western extension of the Raúl mine workings. The location of its trace at the sea level is shown in Figures 2, 3, and 4. The legend is given in Figure 6, and alteration symbols are explained in Figure 3. The section shows the relationship between the unit IV dacite-andesite dome and the nearly coetaneous quartz-diorite porphyry sill-dike complex, with its upper part consisting of a subvolcanic laccolith. These rocks are crosscut by an apophysis of the tonalite 1 stock shown in Figures 3 and 6. Dolerite dikes cut the whole sequence including unit V and are not shown. The alteration zoning and associated copper anomaly follow the same pattern as in Figure 6.

1995) to the end of the Early Cretaceous (end of Albian: 112.2 ± 1.1 Ma, Gradstein et al., 1995). The whole volcanosedimentary sequence is cut by a set of felsic to mafic stocks, dikes, and sills. Figures 6 and 7 show, respectively, a transverse and a longitudinal section through the Raúl-Condestable deposit area.

Lithostratigraphic units

Unit I: Unit I is at least 0.5 km thick in the studied area and consists of submarine basalt, basalt-andesite, tuff, sandstone, and shale. This unit correlates with the Puente Piedra Group described north of Lima where it has a thickness of >2 km (Rivera et al., 1975; Osterman et al., 1983; Injoque, 1985; Salazar and Landa, 1993). This unit is the oldest known from the central Peruvian coast, with fossils giving Berriasian (Rivera et al., 1975), Tithonian to Berriasian (Salazar and Landa, 1993), or Tithonian to early Berriasian ages (Palacios et al., 1992). The term "Asia Formation," introduced by Salazar and Landa (1993) for rocks belonging to the Puente Piedra Group in the Raúl-Condestable deposit area, is not used in this paper. The appearance of quartzite marks the upper limit of this unit and the transition to unit II.

Unit II: Unit II is an ~1.5 km thick clastic sequence consisting of quartzite, sandstone, and shale with minor lava beds. This unit correlates with the Morro Solar Group (Rivera et al., 1975; Salazar and Landa, 1993). Wilson (1963) and Rivera et al. (1975) documented the presence of local limestone, coal, and conglomeratic beds and interpreted this unit as being deposited in a deltaic setting. In the Raúl-Condestable area, no limestone or coal beds are found. Based on the fossil content, the age of the Morro Solar Group is considered to be Valanginian (Salazar and Landa, 1993) or late Berriasian to Valanginian (Palacios et al.,

1992). The disappearance of quartzite and shale and appearance of volcanic rocks marks the transition to unit III.

Unit III: Unit III is 1.3 to >2.5 km thick and consists of a complex sequence of basalt-andesite to andesite, volcanic breccia, tuff, lapillistone, sandstone, bioclastic and oolitic limestone, and shale. This unit shows strong lateral facies and thickness changes as a result of the syndepositional volcanic activity and the complex associated topography. It correlates with the sedimentary Pamplona and Atocongo Formations described in the area of Lima and with the volcano-sedimentary Copará Formation defined to the south in the Ica region (Rivera et al., 1975; Cardozo, 1983; Osterman et al., 1983; Palacios et al., 1992; Salazar and Landa, 1993). It is probable that the Chilca Formation, as defined by Salazar and Landa (1993), is also an equivalent of unit III. Based on the fossil content of the underlying Morro Solar Group (equivalent to unit II), the maximum age of unit III is considered to be late Valanginian, and the youngest is early Aptian (Salazar and Landa, 1993) or early Albian (Palacios et al., 1992).

In the Raúl-Condestable mining operation area, unit III is divided in subunits IIIA to IIID from bottom to top (Fig. 5). This lithostratigraphic subdivision is based on surface, underground, and drilling data combined with previous studies (Ripley and Ohmoto, 1977; Cardozo, 1983; Injoque, 1985). Figure 5 also shows the local lithostratigraphic subdivision used by both geology departments of the Raúl and Condestable mines (unpub. reports for Cía. Minera Pativilca S.A. by R. Flores, 1992, and for Cía. Minera Condestable by J. Zúñiga, 1998). Subunit IIIA lies conformably on unit II. It starts with two calcareous beds intercalated with basalt-andesite and is followed by 300 to 430 m of massive basalt with some volcanic breccia lenses. Subunit IIIA progressively thins a few kilometers to the north of Condestable, whereas its continuation south of the deposit area has not been mapped in detail. Subunit IIIB is 80 to 90 m thick and consists of alternating lapillistone, tuff, and subarkose. This subunit thins out north of the Condestable mine. Farther up in the sequence, the 270- to 360-m-thick subunit IIIC consists of 150 to 195 m of massive porphyritic basalt-andesite lava flows intercalated with seven broadly conformable volcanic breccia beds, overlain by 120 to 165 m of tuff and pyroclastic breccia deposits with subordinate basalt-andesite flows. The upper subunit IIID is about 500 m thick and is characterized by the presence of limestone beds in a sequence dominated by tuff and lava flows at the base, shale, and tuff in the central portion, and finally lava flows and tuff at the top. Limestone beds are bioclastic in the lower and middle part and oolitic in the upper part. All lavas are basalt to basalt-andesite. Bivalves (*Trigonia sp.* and others) and gastropods (*Ampullina sp., Turitella sp.*) are common in bioclastic limestone and tuffaceous beds in the Condestable and Raúl mines. The only identified ammonite (*Olcostephanus cf. asterianus:* Rios, 2000) is from the Condestable mine and corresponds to a late Valanginian to early Hauterivian age (Wright et al., 1996). At about 1 km north from the Condestable mine, unit IIID is less volcanogenic and dominated by shale with intercalations of thin (<1.5 m) limestone beds, which are only slightly recrystallized. These limestone beds are wackestones, rich in oncoids, bivalves, serpulids, bentic foraminifera, and echinoderm plates, indicating deposition under medium- to low-energy conditions, in the photic zone (<50-m water depth). At about the same stratigraphic level, around 2 km southeast from the Raul mine (Cerro Perico; see Fig. 2), Scott and Aleman (1984) reported the presence of a small coral biostrome (*Stylina columbaris*), also indicating deposition in the photic zone. Finally, the presence of oosparite beds at the top of the sequence in the Raúl mine area indicates deposition at water depths of <20 m, which combined with the occurrence of coral biostromes is evidence for a tropical climate at the time of deposition. The upper part of subunit IIID thickens to the northwest (Fig. 3) and grades into an almost purely volcanic sequence devoid of shales and carbonaceous rocks, most probably corresponding to a volcanic edifice. The appearance of quartz-bearing (phenocrystic) lavas marks the transition to unit IV.

Unit IV: Unit IV is 1 to 2 km thick, consisting of quartz-plagioclase-hornblende-phyric massive to flow banded dacitic to andesitic lavas with local autoclastic breccias and no sediment. Lavas of this unit all contain corroded quartz phenocrysts, thus distinguishing them from lavas of other units (Fig. 8A).

The transition to a mafic porphyritic unit (hereafter described as unit V), present in small outcrops located in the southwest of the map area (Fig. 3), marks the top of unit IV. As shown in Figure 6, unit IV corresponds to a 1.5- to 2-km-high dacite-andesite dome, overlying the flanks of the previously described unit IIID basaltic to basalt-andesitic volcanic edifice. No field evidence was found to suggest whether eruption of the unit IV lava dome was submarine or subaerial.

This unit probably corresponds to the upper member of the Quilmaná Group, as described by Salazar and Landa (1993), who assigned to this Group a middle Albian to Late Cretaceous age based on fossils (Fig. 5). The presence of limestone and shale lenses within this dacitic to andesitic lithologic unit indicates deposition under shallow water, at least locally.

Unit V: The bottom of unit V is present southwest from the mine area as small outcrops (Fig. 3). The lithology at the contact consists of a porphyritic basalt-andesite, with plagioclase and altered ferromagnesian phenocrysts in a fine-grained matrix of the same mineralogy with disseminated magnetite (Fig. 8B). Similar outcrops are present west of the mapped area at Cerro Salazar (northwest of Bujama Baja) and on beach outcrops located 2 km south of Bujama Baja (Fig. 2), suggesting a thickness of at least 500 m for this unit.

Unit V might correspond to part of the Casma or Quilmaná Groups, which are considered to be of Albian (Rivera et al., 1975) or Albian to Senonian age (Palacios et al., 1992; Salazar and Landa, 1993).

Intrusive rocks

Leucogabbro: A kilometer-sized leucogabbro intrusion is present in the central part of the quartz-diorite porphyry silldike complex (Fig. 3). It is characterized by a porphyritic texture with plagioclase phenocrysts and by hornblende in rounded glomerophyric aggregates (Fig. 8C). The subordinate matrix consists of a fine-grained mixture of plagioclase and hornblende. This leucogabbro body defines a sill-like structure on top of subunit IIIB and is interpreted to correspond to a subvolcanic intrusion. It is cut by tonalite 1, described below. No clear crosscutting relationships were

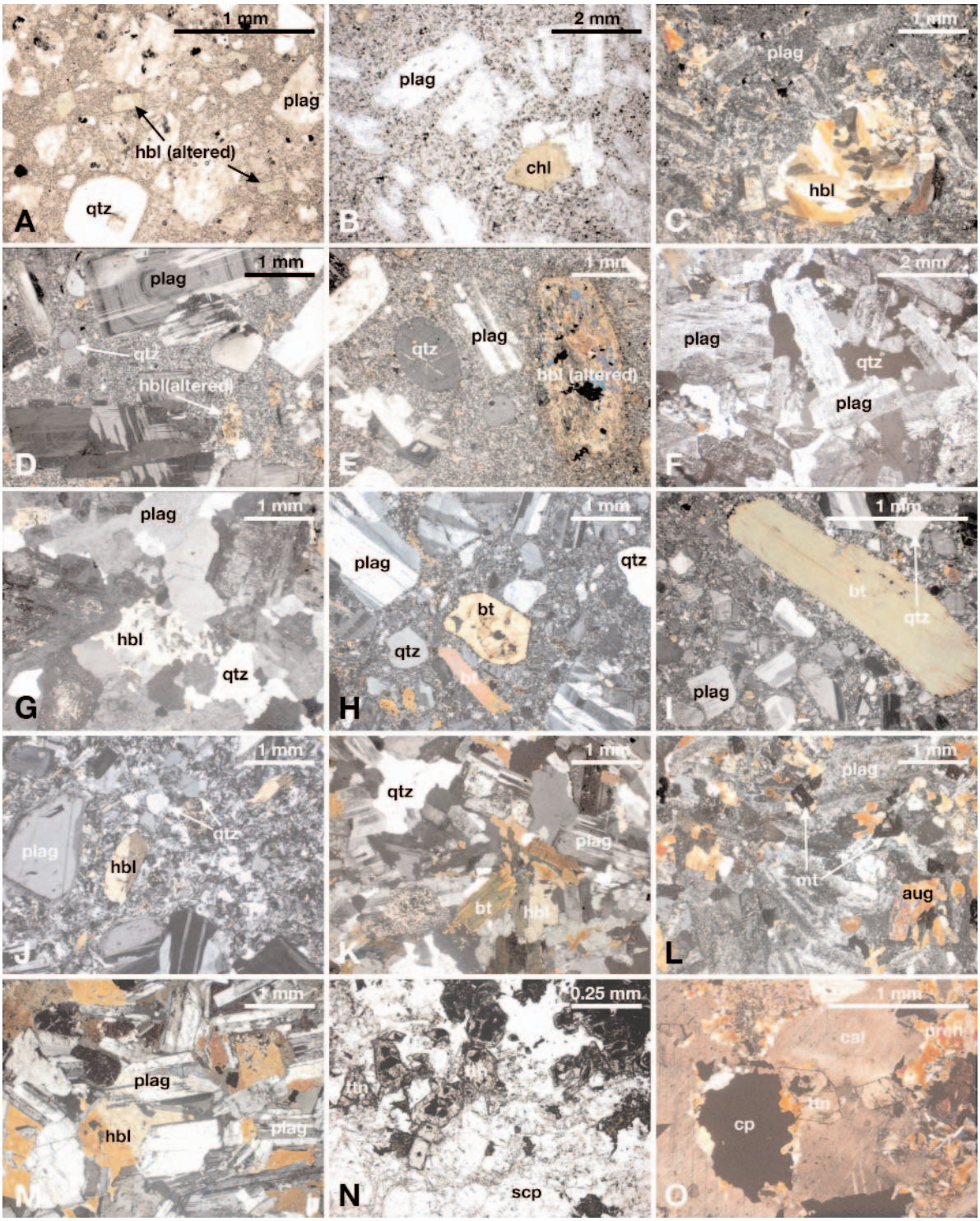

FIG. 8. Photomicrographs of thin sections. A. Unit IV dacite (sample AH-42), showing alteration of Fe chlorite after hornblende and sericite after plagioclase. B. Unit V basalt-andesite (sample AH-138), showing chlorite completely replacing the mafic minerals. C. Leucogabbro (sample AH-75). D. and E. Quartz-diorite porphyry (respectively, samples AH-115 and AH-70), showing alteration of actinolite after hornblende. F. and G. Tonalite 1 (samples AH-8 and AH-111, respectively), showing moderate to week sericitic alteration. H. and I. Tonalite 2 (samples AH-104 and AH-106, respectively). J. Tonalite 3 (sample AH-120). K. Mala tonalite (sample AH-130). L. Dolerite (sample AH-7). M. Gabbro of the Patap superunit (sample AH-2A). N. Titanite crystals in scapolite from the Chilena vein, Raúl mine (sample AH-11). O. Titanite crystals with chalcopyrite and prehnite from the intersection of the Chilena and Pampa veins in the Raúl mine; the calcite is late (sample AH-37). All pictures are in crossed polarizer except A, B, and N. Abbreviations: aug = augite, bt = biotite, cal = calcite, chl = chlorite, cp = chalcopyrite, hbl = hornblende, mt = magnetite, plag = plagioclase, preh = prehnite, qtz = quartz, scp = scapolite, ttn = titanite.

observed with the quartz-diorite porphyry, due to poor surface exposure. An age corresponding to the top of subunit IIIC is considered likely for this lithologic unit.

Quartz-diorite porphyry: The quartz-diorite porphyry contains phenocrysts consisting of zoned plagioclase, hornblende, and corroded quartz, included in a groundmass made up of fine-grained devitrified glass (Fig. 8D-E). The quartz-diorite porphyry sill-dike complex acted as subvolcanic feeder to unit IV volcanic rocks. It crops out over an area of about 3.5 km in diameter. Dikes follow northeast, north-northeast, and northwest orientations. Northeast and north-northeast dikes dip subvertically and steeply southeastward (~82°), respectively, and exhibit minor displacements. In contrast, the northwest-trending Condestable fault dike dips 50° to 45° to the northeast and displays pre- to synintrusion normal movement of up to 500 m (Figs. 3, 6). Most of the sills intrude subunit IIID, with the main and upper sill forming a laccolith structure up to 600 m thick and 4 km long (Figs. 3, 6, 7). This laccolith body is, in part, directly connected through a transition breccia with the overlying coeval unit IV volcanics.

Tonalite 1: Tonalite 1 consists of a stock, 1.6 km long and up to 300 m wide, with minor apophyses that crosscut the center of the quartz-diorite porphyry sill-dike complex (Figs. 3, 6). It is characterized by a medium- to fine-grained texture, consisting of subhedral green hornblende and zoned plagioclase with interstitial quartz (Fig. 8F-G). Tonalite 1 is commonly surrounded by a biotite alteration halo <100 m wide, itself overprinted by a quartz stockwork.

Tonalite 2: Tonalite 2 crops out as a dike about 200 m long and 30 m wide, crosscutting the main tonalite 1 stock (Fig. 3). It is characterized by a medium- to coarse-grained seriate texture with weakly zoned plagioclase, corroded quartz, and biotite (Fig. 8H-I). Broken crystals are common, suggesting a possible explosive emplacement. Biotite alteration is locally associated with the emplacement of tonalite 2.

Tonalite 3: Tonalite 3 crops out northwest of the deposit area, where two intrusions are found. One is a northeast-trending and southeast-dipping dike, 10 to 20 m wide and ≥3 km long, and the other is only known from one roadside outcrop (Fig. 3). Two textural types possibly indicate distinct magmatic pulses or cooling histories. The well-exposed dike is porphyritic, with well-formed brown to green hornblende and plagioclase and rare corroded quartz phenocrysts in a fine-grained seriate to locally granophyric groundmass containing magnetite grains (Fig. 8J). The other is texturally and mineralogically similar to tonalite 1. Tonalite 3 is locally surrounded and partly affected by a halo of biotite alteration, which, in places, grades into quartz-sericite-pyrite alteration.

Mala tonalite: The Mala tonalite crops out outside the studied area, close to the town of Mala (Fig. 2). It is a medium-grained rock with subhedral zoned plagioclase surrounded by anhedral biotite, green hornblende, and quartz (Fig. 8K). Crosscutting relationships with the other intrusive rocks of the area are unknown. Salazar and Landa (1993) included the Mala tonalite in the Jecuan superunit of the Peruvian Coastal batholith, previously defined by Pitcher (1985) and dated by Mukasa and Tilton (1985a) at 101 ± 0.5 Ma (U-Pb in zircon).

Dolerite: All the previously described lithostratigraphic units and intrusive rocks are crosscut by a swarm of dolerite dikes of regional extent (at least tens of kilometers), following the general northwest-southeast Andean trend and dipping 50° to 70° to the northeast in the studied area (Fig. 3). Tectonic movements associated with the emplacement of dolerite dikes are generally less than 10 m. The dolerite is medium grained with seriate to porphyritic texture and local poikilitic domains. It consists of subhedral plagioclase with intergranular to poikilitic augite, skeletal magnetite, and interstitial quartz (Fig. 8L). These dikes are systematically surrounded by a decimeter- to meter-scale halo of epidote alteration.

Patap gabbro: A large gabbroic pluton, tens of km² in surface, belonging to the Patap superunit of the Peruvian Coastal batholith crops out around 8 km east of the Raul-Condestable deposit (Regan, 1985; Salazar and Landa, 1993). This gabbro is medium to coarse grained, with subhedral plagioclase and intergranular hornblende and enstatite (Fig. 8M). Weak to moderate actinolitization of the ferromagnesian minerals and epidotization of the plagioclase are commonly seen. Field observations have shown that blocks previously interpreted as bedrock (Salazar and Landa, 1993) are not in place and belong to a debris flow sourced in the east. Therefore, the limits of the Patap superunit in Figure 2 are shifted 4 km to the east compared to the geologic map (sheet 26-j) of Salazar and Landa (1993).

As previously noted, the age of the Patap superunit is poorly constrained and may span from 84 to 107 Ma (Moore and Agar, 1985; Mukasa and Tilton, 1985a) and more probably from 101.4 to 106 Ma (Mukasa, 1986a).

Geologic setting of the Raúl-Condestable deposit

Fossils and oolititic beds found in unit III are consistent with deposition under shallow seawater conditions, and descriptions by Salazar and Landa (1993) suggest these conditions persisted during the deposition of unit IV (equivalent to the Quilmaná Group). The geology of the deposit area corresponds to a succession of superposed volcanic edifices that were part of a coastal or island volcanic arc. Figure 6 shows that the deposit lies in a subvolcanic position, at 2- to 3-km paleodepth, in the core of a dacitic-andesitic volcanic edifice.

The Raúl-Condestable Ore Deposit

Raul-Condestable deposit is an iron oxide-copper-gold (IOCG) deposit mostly consisting of chalcopyrite and pyrite with pyrrhotite or magnetite (Main ore stage) and crosscut by dolerite dikes. Minor late-stage uneconomic veinlets of calcite-sulfide (sphalerite, galena, chalcopyrite, pyrite, and marcasite) postdate the dolerite dikes emplacement and are not considered to be part of the same hydrothermal event as the Main ore stage (Ripley and Ohmoto, 1977; de Haller et al., 2002). The deposit is centered on the area where the quartz-diorite porphyry and the tonalites intrude, in a subvolcanic position below unit IV (Figs. 3, 4, 6, 7). The mineralization surrounds the stocks of tonalite 1 (and 2) and is mainly developed in unit III. Most of the ore consists of replacement and pore infill that occurred within chemically reactive and/or porous beds (Fig. 5). These include carbonate rocks, tuffs, pyroclastic deposits, and volcanic breccias. The resulting mineralized "mantos" (i.e., orebodies roughly conformable with bedding) and disseminations occur around feeder veins.

These veins trend northeast and northwest and are broadly perpendicular to the bedding. They cut the whole volcanosedimentary sequence from unit II (or possibly lower) to unit IV, including the quartz-diorite porphyry sill-dike complex and, locally, tonalite 1. Mineralization in units II and IV occurs only as veins and no significant mantos or disseminations are known to occur in these lithostratigraphic units.

The alteration pattern (Figs. 3, 4) consists of an early biotite core overprinted by a quartz stockwork, both surrounding but essentially not affecting tonalite 1. The alteration grades outward to an actinolite (± magnetite, ± chlorite, ± titanite, ± scapolite, ± albite, ±epidote) assemblage and upward into a sericite and Fe chlorite assemblage. Actinolite veinlets locally cut the biotite alteration. Prehnite with pumpellyite, in places, overprints the actinolite alteration. An upper distal alteration halo consisting of hematite-chlorite-albite (± epidote, ± calcite) laterally surrounds the sericite + Fe chlorite and the actinolite alteration. The ore is spatially associated with the actinolite alteration and, to a lesser extent, with the sericite + Fe chlorite alteration (Fig. 4).

An interpreted composite paragenetic sequence based on vein and coarse open-space fillings within the main mineralized area is shown in Figure 9 for the Main ore stage. Actinolite and biotite alterations are at least partly coeval with the quartz stockwork and the iron oxides, which occur as open-space fillings and massive replacement. Scapolite occurs as acicular crystals up to 30 cm long within or close to feeder veins. Hydrothermal titanite precipitated together with K-feldspar in veinlets crosscutting scapolite and is commonly found associated with actinolite. Two ore mineral associations which correspond to two end members in terms of redox conditions are distinguished. The oxidized mineral association corresponds to the deposition sequence hematite, magnetite, pyrite, chalcopyrite; the reduced mineral association corresponds to the sequence pyrrhotite, pyrite, chalcopyrite. The oxidized mineral association is mostly found in veins and replacing limestone of subunit IIID, whereas the reduced mineral association is common in subunits IIIC and IIID as veins and breccias. In the oxidized mineral association, magnetite is completely pseudomorphous and overgrown by hematite. Minor molybdenite is found, locally, in the reduced mineral association. Both sequences end with pyrite followed by chalcopyrite, with minor sphalerite and galena. Gold occurs as inclusions within chalcopyrite. Prehnite and pumpellyite are late compared to sulfides and are found in or close to feeder veins. Zoning is recognized in both veins and mantos, with the following minerals occurring proximal to distal relative to the feeder veins: chalcopyrite-pyrite-magnetite for the oxidized mineral association and chalcopyrite-pyrite-pyrrhotite for the reduced mineral association. The zoning from chalcopyrite to magnetite or pyrrhotite also corresponds to a late to early position in the paragenetic sequence (Fig. 9) and can be observed at scales of tens of meters.

High-salinity fluid inclusions are found in the quartz stockwork veins surrounding the tonalites 1 and 2 but also in magmatic quartz of tonalite 1 (de Haller et al., 2002; de Haller, 2006). These inclusions commonly contain a vapor bubble, together with halite and iron chloride daughter crystals (determination by EDS). They are associated with two-phase inclusions (V + L) and vapor-rich inclusions.

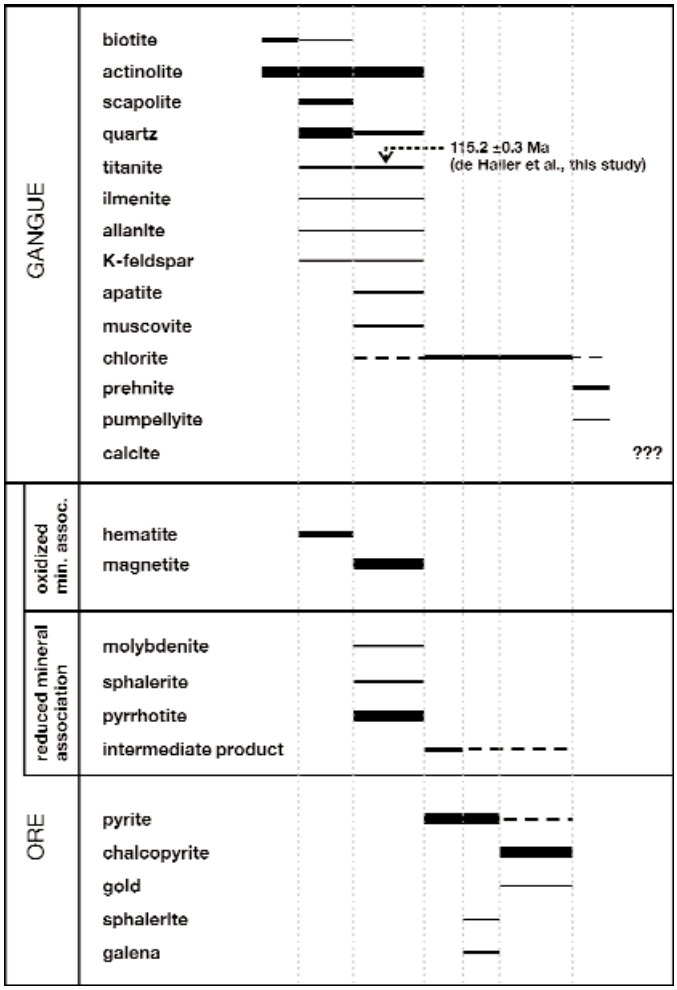

FIG. 9. Interpreted paragenetic sequence of the Main ore stage (IOCG stage). The sequence is based on vein and coarse open-space fillings within the main mineralized area. The late (post-dolerite emplacement) calcite sulfides vein stage is not shown.

The sulfur isotope compositions of the Main ore stage sulfides range from 2.7 to 26.3 per mil CDT (de Haller et al., 2002; de Haller, 2006), but values as low as –5 per mil have been reported (Ripley and Ohmoto, 1977). The majority of the values are close to 5 per mil. These data are consistent with a magmatic source of sulfur, and the highly positive values have been interpreted to reflect an external source of thermally reduced sulfur from seawater or evaporite (Ripley and Ohmoto, 1977; de Haller et al., 2002). In contrast, late-stage sulfides from the calcite veinlets have strongly negative $\delta^{34}S$ values, ranging between –31.1 and –22.9 per mil, suggesting the incorporation of reduced sulfur from sedimentary rocks (de Haller et al., 2002).

Whole-Rock Geochemistry of Magmatic Rocks

Major and trace element results for selected representative samples of lava, tuff, and intrusions of the Raúl-Condestable area are presented in Table 1, and the complete dataset is provided as a digital supplement to this paper at www.segweb.org. Because important hydrothermal circulation occurred in the area of the deposit, most of the rocks are

moderately to intensely altered. Therefore, discriminant diagrams, such as the TAS (total alkali-silica) diagram of Le Bas et al. (1986), cannot be used. Some trace or minor elements, such as Ti, Zr, Y, and Nb, are known to be essentially immobile in the great majority of hydrothermal and metamorphic environments and can be assumed to be immobile in the great majority of the studied samples. Samples with quartz stockwork, obvious silicification or LOI greater than 5 percent, reflecting late carbonate are not considered.

Figure 10A-D shows the Zr/TiO_2 versus Nb/Y and SiO_2 versus Zr/TiO_2 ratios diagrams (cf. Winchester and Floyd, 1977). The plotted data were normalized to 100 percent on an anhydrous basis by removing the LOI. Near immobility of silica in Figure 10C and D can be assumed from the diagrams of TiO_2 versus SiO_2 and Zr versus SiO_2 (Fig. 10E-F), in which felsic rocks plot in well-defined trends, independently of the intensity and nature of the alteration. Figure 10A-D gives similar and coherent results, with all the rocks plotting in the

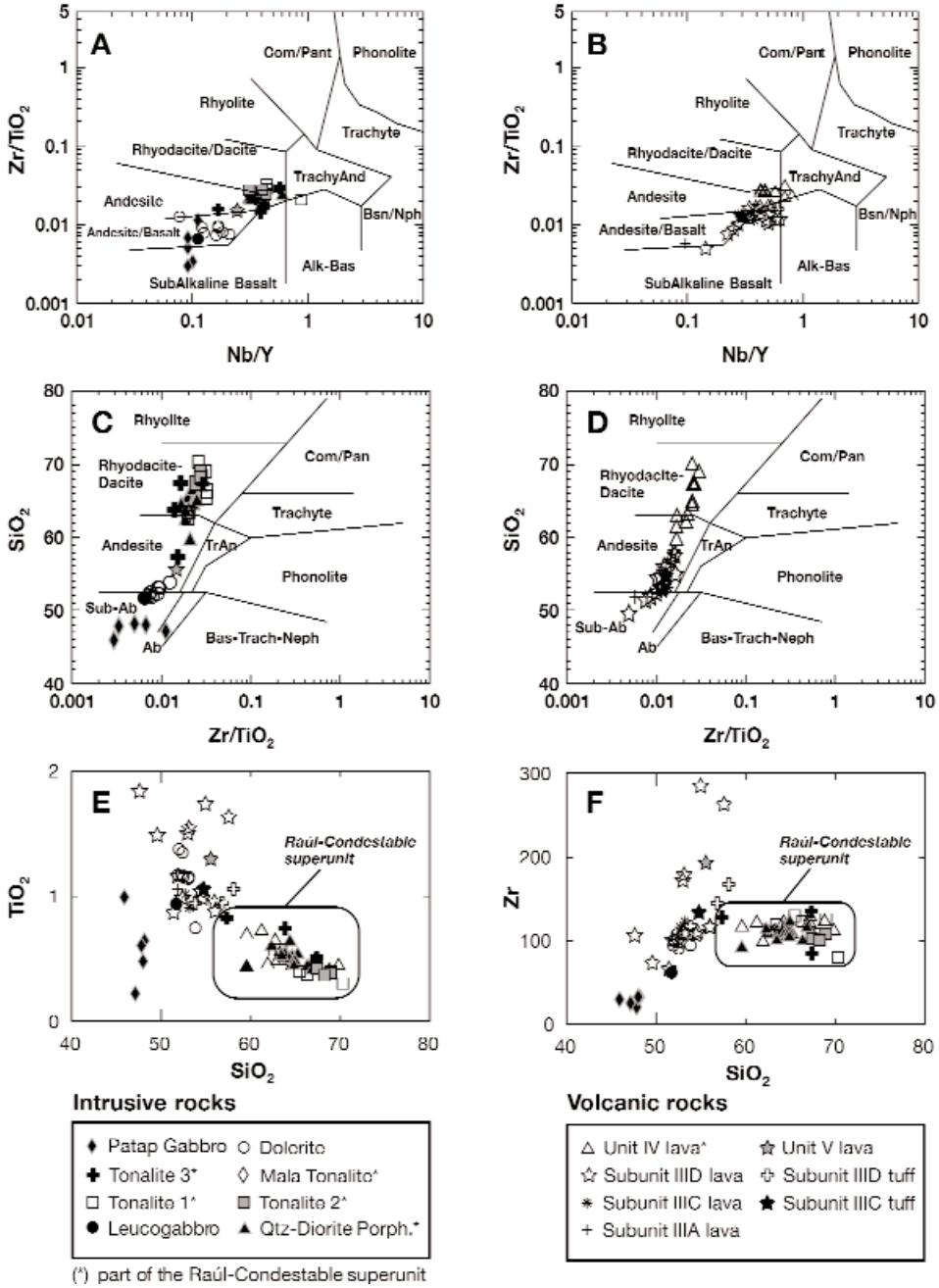

FIG. 10. Geochemical discrimination diagrams for igneous rocks of the Raúl-Condestable area. The plotted data are provided in a digital supplement to this paper at www.segweb.org. All the values are normalized to 100 percent on a dry basis. Diagrams A to D from Winchester and Floyd (1977). Diagrams E and F show that TiO_2, Zr, and SiO_2 in felsic rocks of the Raúl-Condestable superunit were mostly immobile. Diagrams E and F also show the distinct TiO_2 and Zr vs. SiO_2 trend of the Raúl-Condestable superunit compared with the magmatic rocks of other units (see text).

subalkaline field. Whereas felsic rocks (quartz-diorite porphyry, unit IV lava, and tonalites) mostly plot in the dacite field of the SiO_2 versus Zr/TiO_2 diagram (Fig. 10C-D), they mainly fall within the andesite field of the Zr/TiO_2 versus Nb/Y diagrams (Fig. 10A-B). This is explained by the fact that the differentiation trend (TiO_2 depletion in Fig. 10E) is not accompanied by a concomitant Zr enrichment (Fig. 10F), a behavior consistent with amphibole (± biotite and zircon) fractionation during differentiation (Pearce and Norry, 1979). Thus, a classification based on the silica content is considered more reliable than the Zr/TiO_2 ratio, and the volcanic rocks of unit IV, the quartz-diorite porphyry, and the tonalites are considered to be mostly dacitic (Fig. 10C, D).

In the ternary diagrams of Figure 11A-D, basaltic samples plot in the volcanic arc field (either calc-alkaline or tholeiitic), with a MORB affiliation indicated for some samples. The MORB-normalized spider diagram (Fig. 11E) of Pearce (1983) has been applied to the three least altered basaltic

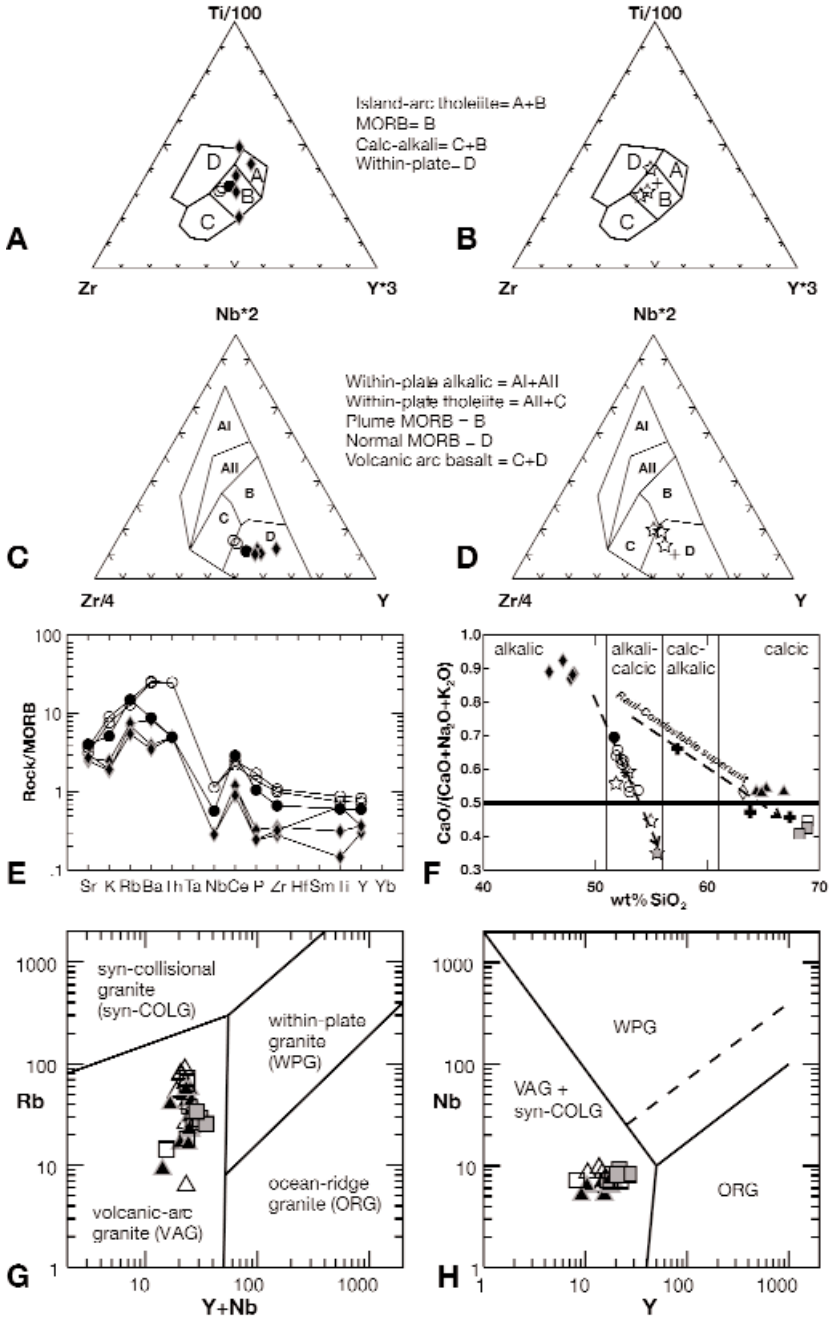

FIG. 11. Geochemical discrimination diagrams of tectonic settings of igneous rocks from the Raúl-Condestable area. Symbols are the same as the ones used in Figure 10. The plotted data are provided in a digital supplement to this paper at www.segweb.org. Only least altered samples were used in diagrams E and F. All the values are normalized to 100 percent on a dry basis. Diagrams A and B are from Pearce and Cann (1973), C and D from Meschede (1986), E from Pearce (1983), F modified from Peacock (1931), and G and H from Pearce et al. (1984). See text for explanation.

rocks of the Raúl-Condestable area: the leucogabbro, the Patap Gabbro, and the dolerite. These rocks are enriched in the alkali and alkaline earth elements, but also in Th, and, to a lesser extent, Ce. In contrast, Nb, P, Zr, Ti, and Y are depleted to various degrees relative to MORB. The shape of the plot is typical of basalt from a subduction setting (Pearce, 1983) and excludes both within-plate and MORB contexts. The enrichment from Sr to Th is directly related to the metasomatism that occurs in the mantle due to slab dehydration. All the samples display a near-horizontal profile for the elements Nb, Zr, Ti, and Y, which, according to Pearce (1983) could mean that the volcanic arc in the Raúl-Condestable area developed on a basement consisting of oceanic crust.

Tonalites 1 and 2 and Mala tonalite samples all cluster in the volcanic arc granite field of Figure 11G (VAG), and volcanic arc granite-syncollisional granite field of Figure 11H (VAG + syn-COLG). Although alteration, and particularly the sericite-chlorite assemblage, might increase the Rb content of the rocks, this is not apparent in Figure 11G, as all the samples including the quartz-diorite porphyry and the unit IV dacite-andesite cluster in the VAG field.

Pb Isotopes

Lead isotope compositions of main ore-stage sulfides, late vein sulfides, and tonalites 1 and 2 (whole-rock values corrected for age; Table 2, Fig. 12) fall on a mixing trend between Nazca plate MORB and Pacific Ocean sediments and Mn nodule fields, in good agreement with previous data and interpretations of Mukasa (1986b), Gunnesh et al. (1990), and Mukasa et al. (1990). Assimilation of Precambrian lead (Arequipa Massif field in Fig. 12) observed farther south in the Peruvian Coastal batholith (field I in Fig. 12: Mukasa, 1986b) can be ruled out in the Raúl-Condestable area.

U-Pb and Hf Isotope Data: Results and Interpretation

Zircon U-Pb dating was completed on unit IV dacite, quartz-diorite porphyry, tonalite 1, tonalite 2, and Mala tonalite. Additionally, U-Pb dating of hydrothermal titanite was performed on two vein samples. Zircons are euhedral and colorless, and hydrothermal titanite is pale brown and transparent. When observed under cathodoluminescence (Fig. 13), all zircons showed oscillatory and sector zoning that is typically igneous (Hoskin and Schaltegger, 2003). There was no evidence for old inherited zircon cores (Corfu et al., 2003). Rare zircons from the quartz-diorite porphyry and the Mala tonalite (see Fig. 13F) contain domains that may have undergone subsolidus recrystallization (Corfu et al., 2003; Hoskin and Schaltegger, 2003), as shown by green luminescent lobate embayments overprinting the oscillatory zoning. These features are difficult to interpret, but they differ from that of typical inherited xenocrysts. Bright yellow-green luminescent fringes are commonly observed on the periphery of the crystals (mostly at the pyramidal terminations), which could suggest some local recrystallization. Recrystallization purges the crystal from nonessential structural constituent cations (like Pb), which have ionic radii significantly different from those of Zr and Si, and this could cause Pb loss (Hoskin and Schaltegger, 2003). The zircon abrasion process used in the analytical procedure normally removes this recrystallized material (Krogh, 1982).

Table 3 gives all the U-Pb and Hf isotope results, and concordia plots are shown in Figure 14. In Figure 15 the ε_{Hf}(115 Ma) data are plotted versus the $^{206}Pb/^{238}U$ ages. Sample locations are given in Figures 2 and 3. All the U-Pb data points are concordant but not all may correspond to an actual crystallization event. Each sample shows a slight dispersion along the concordia curve that in most cases can be attributed to Pb loss. One fraction of zircon from tonalite 1 (O40/17 in Table 3), analyzed without abrasion to test the Pb-loss hypothesis, yielded a slightly discordant data point with the youngest apparent age of the group (see below and Fig. 14), thus supporting the inference that the dispersion in ages can be related to superficial Pb loss and insufficient abrasion. Because of this, the age interpretations discussed below are weighed

Table 2. Pb Isotope Data of Sulfides and Whole Rocks from the Raúl-Condestable Deposit

Sample	Mineral/rock	Hydrothermal stage	Pb/Pb ratios[1]			Corrected to 115 Ma[2]		
			$^{206}Pb/^{204}Pb$	$^{207}Pb/^{204}Pb$	$^{208}Pb/^{204}Pb$	$^{206}Pb/^{204}Pb$	$^{207}Pb/^{204}Pb$	$^{208}Pb/^{204}Pb$
AH-16	Pyrite 1[3]	IOCG[2]	18.594	15.656	38.602			
AH-16	Pyrite 2[3]	IOCG[2]	18.590	15.648	38.558			
AH-34	Pyrite	IOCG[2]	18.597	15.655	38.583			
AH-81	Pyrite	IOCG[2]	18.636	15.639	38.546			
AH-84	Pyrite	IOCG[2]	18.612	15.661	38.595			
AH-11	Galena	Late veins?[4]	18.576	15.629	38.507			
AH-13	Galena	Late veins[4]	18.609	15.631	38.510			
AH-18	Pyrite	Late veins[4]	18.580	15.635	38.518			
AH-8	Tonalite 1		18.802	15.664	38.713	18.512	15.650	38.524
AH-40	Tonalite 1		18.844	15.689	39.029	18.511	15.673	38.650
AH-104	Tonalite 2		18.784	15.574	38.867	18.495	15.560	38.489
AH-106	Tonalite 2		18.862	15.581	39.049	18.513	15.564	38.822

[1] The analytical uncertainties (2s) are 0.05 percent for $^{206}Pb/^{204}Pb$, 0.08 percent for $^{207}Pb/^{204}Pb$ and 0.10 percent for $^{208}Pb/^{204}Pb$

[2] Using XRF results for U, Pb, and Th (see Table 1 and digital supplement)

[3] Pyrite 2 is paragenetically later than pyrite 1

[4] IOCG = iron oxide copper-gold stage, or Main ore stage (pre-dolerite emplacement); late veins = late-stage calcite sulfide veins (post-dolerite emplacement)

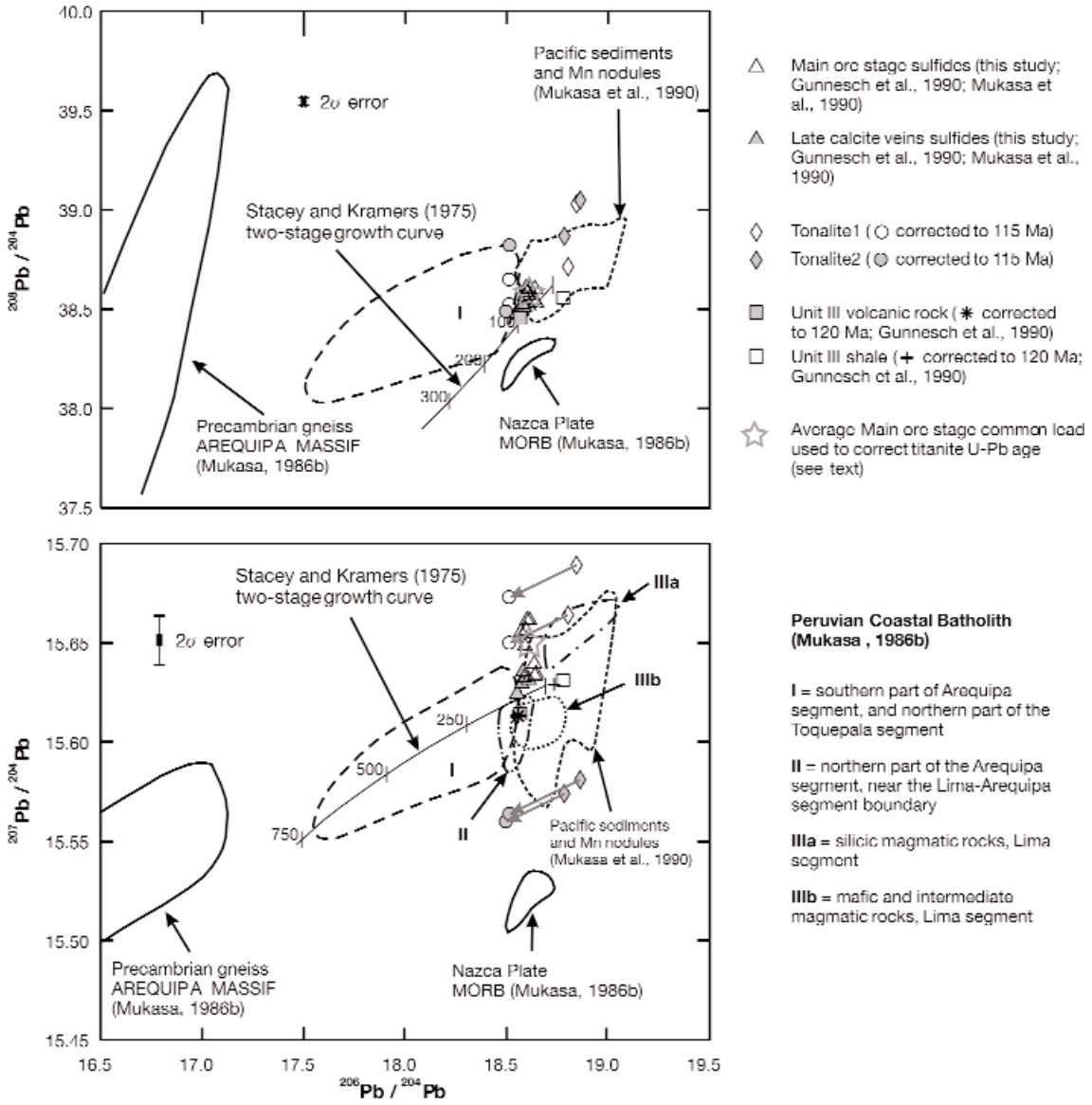

FIG. 12. Plots of sulfide and whole-rock Pb isotope data of samples from the Raúl-Condestable deposit area. Plotted data include results from Gunnesch et al. (1990) and Mukasa et al. (1990). Main ore stage sulfides correspond to the IOCG mineralization itself (pre-dolerite emplacement) and are distinguished from the late-stage calcite sulfide veins (post-dolerite emplacement). Rocks of the northern part of the Arequipa segment and from the Lima segment of the Peruvian Coastal batholith mostly fall between the Pacific sediments and Mn nodules and the Nazca plate MORB (Mukasa, 1986b; Mukasa et al., 1990). In contrast, rocks from the southern part of the Arequipa segment show assimilation of Pb from the Precambrian Arequipa Massif. Pb isotope data from samples of the Raúl-Condestable deposit area (sulfides and whole rock) do not indicate assimilation of Precambrian basement.

most strongly in favor of the oldest data points in any one group. All the given errors are at 95 percent certainty. Hafnium isotopes were analyzed on each dated zircon fraction to constrain the nature of the magma source (e.g., Faure, 1986). The isotope ^{176}Hf results from the decay of ^{176}Lu, and the ratio $^{176}Hf/^{177}Hf$ depends on the age of the sample and on its initial Lu/Hf ratio. Lu is more refractory than Hf and is partitioned into the mantle, whereas Hf is enriched into the crust. Since zircons contain significant amounts of Hf (on the order of 10,000 ppm) but very low contents of Lu (about 24 ppm), their $^{176}Hf/^{177}Hf$ ratio nearly corresponds to the isotope ratio of the magma at the time of crystallization. Positive $\varepsilon Hf(T)$ indicate a dominance of depleted mantle component, whereas negative $\varepsilon Hf(T)$ indicate a dominantly crustal contribution.

Unit IV dacite

Five U-Pb analyses of zircon (sample AH-42; Figs. 3, 8A) spread over a 2- to 3-m.y. interval along the concordia curve (Fig. 14). A correlation exists between the different zircon morphologies and the age, with the short prismatic crystals giving the youngest ages, the broken tips intermediate ages,

TABLE 3. U-Pb and Hf Isotope Data of Magmatic Zircons and

		Concentrations[1]						Atomic ratios				
Sample no.	Description[3]	Weight (μg)	*n* of grains	U (ppm)	Pb_{ic}[4] (ppm)	Pb_c[4] (pg)	Th/U[5]	206/204[6]	206/238[7,8]	Error 2σ (abs.)	0.0879	Error 2σ (abs.)
AH-42	Unit IV dacite (UTM coordinates: 326234E, 8594423N); the sample alteration consists of total chloritization of the hornblende and strong											
O37/18	Z tips	97	59	83	0.00	2.4	0.54	3792	0.01811	0.00005	0.12043	0.00046
O37/19	Z lp	90	27	71	0.11	11.5	0.61	649	0.01826	0.00006	0.12080	0.00101
O40/2	Z tips	45	19	95	0.01	2.3	0.52	2127	0.01808	0.00006	0.12029	0.00058
O40/20	Z sp	50	>50	131	0.00	1.8	0.52	4110	0.01793	0.00008	0.11967	0.00056
O44/12	Z sp LT	19	14	124	0.16	4.9	0.55	556	0.01796	0.00005	0.11932	0.00096
AH-115	Qtz-diorite porphyry (UTM coordinates: 328950E, 8595500N); the sample alteration consists of actinolite and minor chlorite after hornblende,											
O37/13	Z tips	12	27	83	0.27	5.2	0.42	238	0.01828	0.00006	0.12189	0.00226
O37/14	Z sp	25	13	72	0.06	3.5	0.50	613	0.01820	0.00005	0.12036	0.00116
O37/15	Z lp	13	12	130	0.00	1.4	0.47	1391	0.01822	0.00006	0.12099	0.00082
O40/13	Z tips	33	>50	116	0.08	4.7	0.43	943	0.01821	0.00006	0.12161	0.00072
O40/14	Z whole sp-lp	57	40	117	0.00	2.1	0.40	3683	0.01810	0.00005	0.12057	0.00045
AH-8	Tonalite 1 (UTM coordinates: 328045E, 8595509N); the sample is moderately altered, with chlorite, actinolite, and minor titanite and epidote											
O37/16	Z lp	55	50	52	0.00	1.9	0.51	1675	0.01796	0.00005	0.11931	0.00070
O37/17	Z tips (pa)	13	5	82	0.00	1.4	0.46	881	0.01764	0.00005	0.11745	0.00113
O37/24	Z sp	92	30	42	0.04	5.3	0.50	848	0.01801	0.00004	0.11975	0.00073
O40/15	Z tips	167	>50	66	0.02	5.2	0.47	2337	0.01765	0.00006	0.11763	0.00053
O40/16	Z sp	55	>50	80	0.00	1.8	0.52	2716	0.01792	0.00004	0.11916	0.00050
O40/17	Z lp (na)	124	>50	120	0.03	5.7	0.42	2857	0.01744	0.00005	0.11651	0.00042
AH-104	Tonalite 2 (UTM coordinates: 327975E, 8595550N); the sample is weakly altered, with chlorite after biotite and rare patches of epidote and											
O37/20	Z tips	56	>50	47	0.00	1.8	0.47	1666	0.01810	0.00005	0.12043	0.00069
O37/21A								----------	----------	----------	----------	no data ----------
O37/21B	Z lp (in)	174	33	40	0.00	2.7	0.47	2998	0.01797	0.00006	0.11959	0.00052
O40/18	Z sp	123	>50	55	0.01	3.7	0.47	2016	0.01769	0.00005	0.11793	0.00048
O40/19	Z sp (in)	201	>50	52	0.10	21.3	0.45	557	0.01765	0.00006	0.11743	0.00088
O44/10	Z sp HA	31	30	50	0.00	1.6	0.51	1136	0.01803	0.00006	0.11968	0.00098
O44/11	Z tips	60	47	60	0.04	4.6	0.45	890	0.01798	0.00005	0.11955	0.00072
AH-130	Mala tonalite (UTM coordinates: 323575E, 8600825N); the sample is weackly altered, with chlorite after both biotite and hornblende, and											
O37/22	Z sp	32	40	27	0.02	2.6	0.45	396	0.01799	0.00006	0.11946	0.00204
O37/23	Z mp	66	22	40	0.10	8.8	0.66	350	0.01781	0.00006	0.11709	0.00144
O40/21	Z lp-sp-tips (in)	170	>50	48	0.05	11.0	0.53	855	0.01791	0.00005	0.11902	0.00067
O40/22	Z eq-sp (in)	80	>50	53	0.41	34.7	0.47	158	0.01821	0.00007	0.12288	0.00294
AH-11	IOCG titanite (Chilena vein, block T-448, level -120 (6 m above sea level), Raúl mine; UTM coordinates: 327770E, 8595154N)											
O37/S.1	T	10	5	103	3.41	38.5	0.30	48.6	0.01799	0.00007	0.1132	0.0069
O45/S.FC3	T	144	50	77	1.21	180.8	0.32	86.2	0.01769	0.00006	0.1164	0.0024
AH-37	IOCG titanite (Chilena and Pampa veins intersection, block T-630, level -30 (94 m above sea level), Raúl mine; UTM coordinates: 328035E,											
O45/S.FC6	T (alt)	71	11	57	0.32	32.5	0.19	160	0.01805	0.00006	0.1181	0.0023
O49/S.3	T na	317	37	49	0.23	82.4	0.14	232	0.01800	0.00005	0.1198	0.0011
O49/S.4	T	323	40	40	0.30	104.4	0.16	159	0.01801	0.00005	0.1206	0.0015
O49/S.5	T (alt)	171	30	29	0.25	51.4	0.22	127	0.01802	0.00006	0.1212	0.0027

-- = no data

[1] weight and concentrations are known to better than 10%

[2] 176Hf/177Hf(115Ma) are with 2σ internal errors, and εHf(115Ma) are with 2σ external errors

[3] Z = zircon (euhedral, colorless, free of fractures and inclusions unless otherwise indicated); sp = short prismatic (l/w = 1-3); mp = middle-prismatic (l/w alt = local alteration persisting after abrasion; na = nonabraded (all the others abraded); pa = poorly abraded

[4] Pbic = total (initial) common Pb after correction for blank; Pbc = total common Pb in sample (initial +blank)

[5] Th/U model ratio inferred from 208/206 ratio and age of sample

[6] raw data corrected for fractionation and blank

[7] Corrected for fractionation, spike, blank and initial common Pb (corrected using composition estimated from Stacey and Kramers, 1975, model in uncertainty

[8] Corrected for initial Th disequilibrium, using an estimated Th/U ratio of 4 for the melt

Hydrothermal Titanite from the Raúl-Condestable Deposit

		Apparent ages [Ma]							Hf data[2]			
207/206[7,8]	Error 2σ (abs.)	206/238[7,8]	Error 2σ (abs.)	0.1	Error 2σ (abs.)	207/206[7,8]	Error 2σ (abs.)	Error corr.	$^{176}Hf/^{177}Hf$ (115 Ma)	Error 2σ (abs.)	εHf (115 Ma)	Error 2σ (abs.)
sericitization and weak carbonatization and epidotization of the plagioclase												
0.04823	0.00011	115.7	0.3	115.5	0.4	110	6	0.79	0.282835	3	5.2	0.5
0.04798	0.00035	116.7	0.4	115.8	0.9	98	17	0.47	0.282833	3	5.1	0.5
0.04826	0.00017	115.5	0.4	115.3	0.5	112	8	0.70	0.282838	3	5.3	0.7
0.04842	0.00015	114.5	0.5	114.8	0.5	120	7	0.78	0.282831	2	5.1	0.7
0.04819	0.00034	114.7	0.3	114.5	0.9	109	17	0.50	0.282837	3	5.3	0.7
with plagioclase being only weakly sericitized												
0.04836	0.00085	116.8	0.4	116.8	2.0	117	41	0.40	0.282849	5	5.7	0.5
0.04796	0.00041	116.3	0.3	115.4	1.1	97	20	0.48	0.282856	4	5.9	0.5
0.04816	0.00028	116.4	0.4	116.0	0.7	107	14	0.54	0.282875	3	6.6	0.5
0.04844	0.00023	116.3	0.4	116.5	0.6	121	11	0.62	0.282863	6	6.2	0.7
0.04833	0.00012	115.6	0.3	115.6	0.4	115	6	0.75	0.282842	4	5.4	0.7
after hornblende, sericite after plagioclase, and carbonate												
0.04819	0.00023	114.7	0.3	114.4	0.6	109	11	0.61	0.282873	4	6.5	0.5
0.04828	0.00042	112.7	0.3	112.8	1.0	113	21	0.44	0.282905	9	7.7	0.5
0.04823	0.00025	115.0	0.3	114.8	0.7	111	12	0.55	0.282869	3	6.4	0.7
0.04834	0.00013	112.8	0.4	112.9	0.5	116	6	0.82	0.282868	2	6.4	0.7
0.04823	0.00015	114.5	0.3	114.3	0.5	111	7	0.69	0.282872	5	6.5	0.7
0.04845	0.00010	111.5	0.3	111.9	0.4	121	5	0.82	0.282882	3	6.9	0.7
carbonatization												
0.04826	0.00022	115.6	0.3	115.5	0.6	112	11	0.59	0.282879	3	6.8	0.5
----------									0.282884	3	6.9	0.5
0.04825	0.00015	114.8	0.4	114.7	0.5	112	7	0.70	0.282874	4	6.6	0.5
0.04834	0.00013	113.1	0.3	113.2	0.4	116	6	0.76	--	--	--	--
0.04825	0.00031	112.8	0.4	112.7	0.8	111	15	0.50	0.282882	2	6.9	0.7
0.04813	0.00034	115.2	0.4	114.8	0.9	106	16	0.53	0.282874	3	6.6	0.7
0.04823	0.00024	114.9	0.3	114.7	0.7	111	12	0.59	0.282872	2	6.5	0.7
sericite (± epidote) after plagioclase												
0.04816	0.00077	114.9	0.4	114.6	1.8	107	37	0.41	0.282893	2	7.3	0.5
0.04767	0.00054	113.8	0.4	112.4	1.3	83	27	0.41	0.282898	2	7.4	0.5
0.04819	0.00021	114.4	0.3	114.2	0.6	109	10	0.63	0.282903	3	7.6	0.7
0.04894	0.00115	116.3	0.4	117.7	2.7	145	54	0.20	0.282893	2	7.3	0.7
0.04563	0.00263	115.0	0.5	108.9	6.3	--	--	0.82				
0.04774	0.00092	113.0	0.4	111.8	2.2	87	45	0.59				
8595011N)												
0.04743	0.00087	115.3	0.4	113.3	2.1	71	43	0.51				
0.04825	0.00040	115.0	0.3	114.9	1.0	111	20	0.54				
0.04858	0.00052	115.1	0.3	115.7	1.3	128	25	0.59				
0.04878	0.00102	115.1	0.4	116.1	2.5	137	48	0.55				

= 3-4); lp = long-prismatic (l/w >4); LT,HA = low T, high A typological index (Pupin, 1980); in = inclusions; T = titanite (pale-brown, transparent grains);

zircon and using average Pb compositions of pyrite from IOCG hydrothermal stage for titanite); error calculated by propagating the main sources of

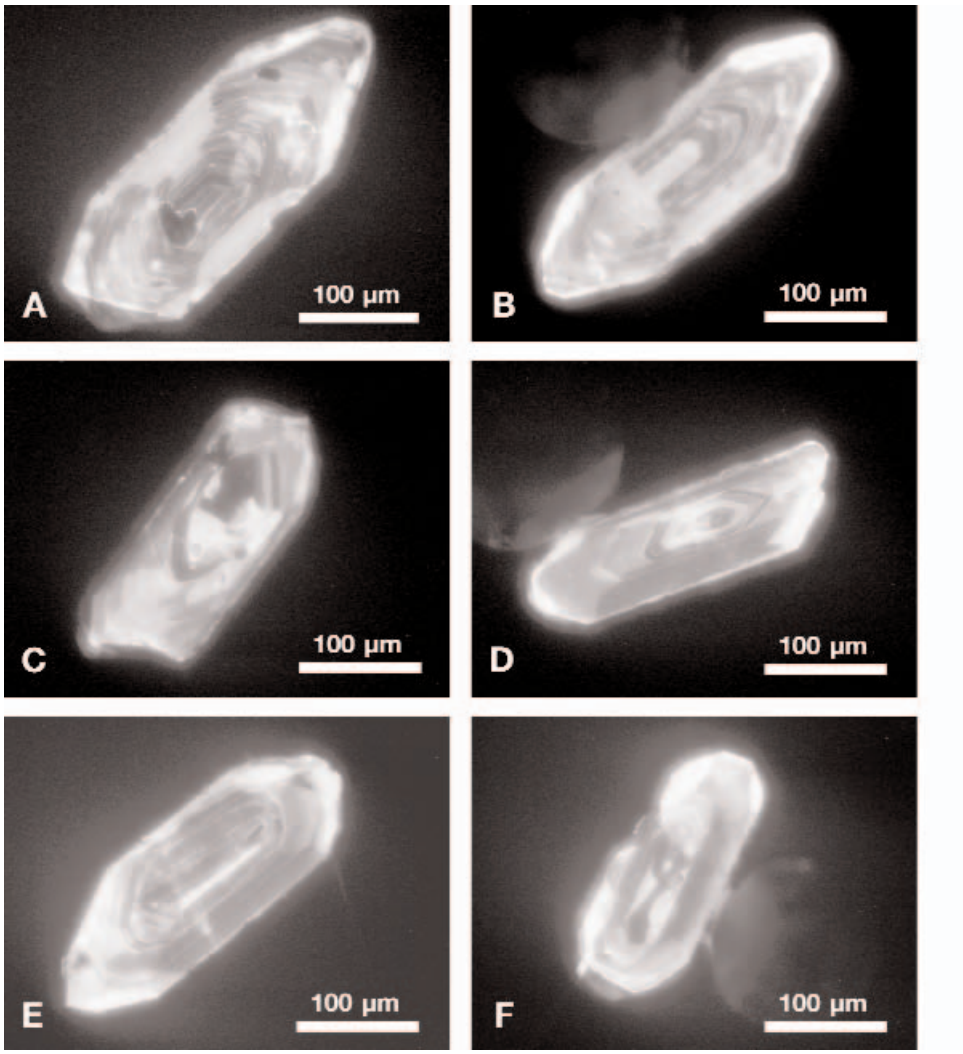

FIG. 13. Cathodoluminescence photomicrographs of zircons from dated samples. A. Unit IV dacite (sample AH-42). B. Quartz-diorite porphyry (sample AH-115). C. Tonalite 1 (sample AH-8). D. Tonalite 2 (sample AH-104). E and F. Mala tonalite (sample AH-130). Pictures were taken on polished sections with a Technosyn 8200 MkII cathodoluminescence microscope working at 15 kV and 575 to 595 μA with a vacuum of 0.1 Torr.

and the long prismatic zircons the oldest ages. There is also an inverse correlation between the U content and both the average size of the grains (fraction weight/number of grains) and the $^{206}Pb/^{238}U$ age, reflecting the well-known relationship between discordance induced by Pb loss and zircon properties (Silver and Deutsch, 1963). Thus, the 116.7 ± 0.4 Ma $^{206}Pb/^{238}U$ age of the oldest analyzed zircon is considered to most closely represent the time of emplacement of the unit IV dacite. The Hf isotope results are very homogeneous ranging from ε_{Hf}(115 Ma) = 5.1 to 5.3, with a weighted average of 5.2 ± 0.3 (Fig. 15, Table 3).

Quartz-diorite porphyry

In the concordia plot (Fig. 14), four of five zircon analyses (sample AH-115; Figs. 3, 8D) overlap, giving an age of 116.4 ± 0.3 Ma. The fifth analysis is slightly younger due to probable Pb loss and is not considered in the age calculation. Values of ε_{Hf}(115 Ma) range from 5.5 to 6.6, with a weighted average of 6.0 ± 0.6 (Fig. 15, Table 3).

Tonalite 1

In the concordia plot (Fig. 14), a group of three fractions of zircon from sample AH-8 (Figs. 3, 8F) yield the oldest age of 114.8 ± 0.4 Ma, which is considered the true age of tonalite 1. Two slightly younger analyses are interpreted as being partially affected by Pb loss, as suggested by the position and youngest apparent age of the nonabraded zircon analysis. All but one of the ε_{Hf}(115 Ma) values are grouped between 6.4 and 6.9 giving a weighted average of 6.5 ± 0.3 (Fig. 15, Table 3). The cause of the outlier at 7.7 is unknown.

Tonalite 2

Four zircon analyses from sample AH-104 (Figs. 3, 8H) are clustered in a group with a common age of 115.1 ± 0.4 Ma (Fig. 14). Two other fractions plotting between 114 and 112 Ma are considered to have been affected by lead loss. The six ε_{Hf}(115 Ma) results are grouped between 6.5 and 6.9, averaging 6.7 ± 0.2 (Fig. 15, Table 3).

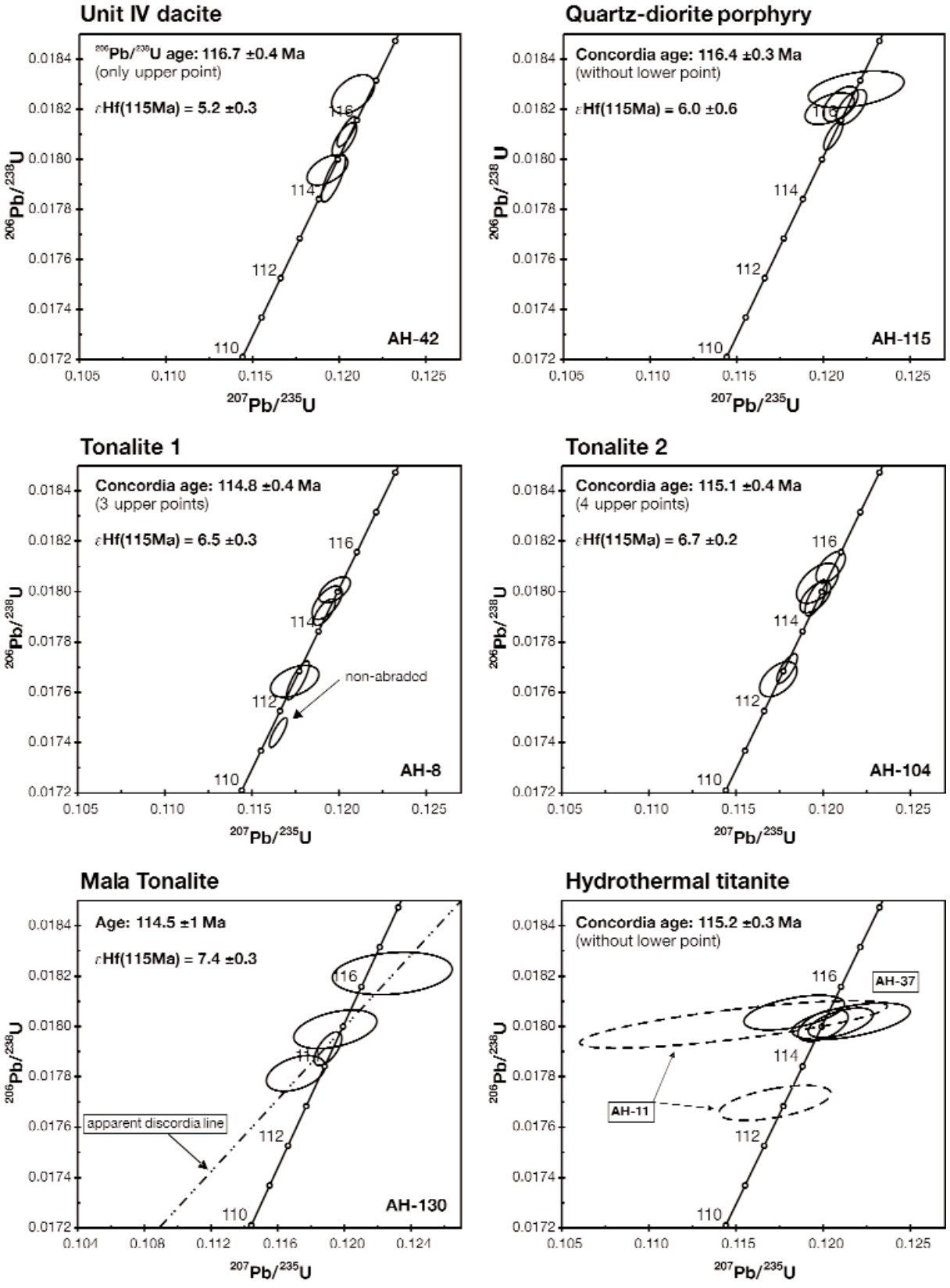

FIG. 14. U-Pb concordia plots of dated zircon and titanite (Table 3). Plots, ages, and errors were calculated with the ISOPLOT program of Ludwig (1999). Data point error ellipses are 2σ. The ε_{Hf}(115Ma) values were calculated from the Hf isotope values obtained on the dated zircons (Table 3). Uncertainties on the ages and Hf values represent the 95 percent confidence level.

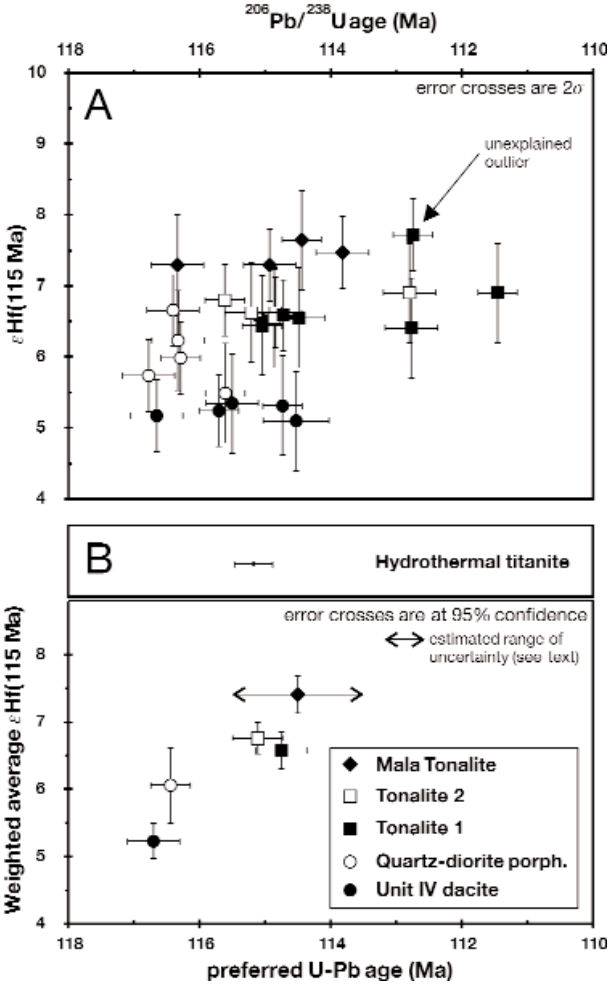

FIG. 15. Plots of ε_{Hf}(115Ma) vs. U-Pb ages of the dated zircons. A. Plot of ε_{Hf}(115Ma) vs. the $^{206}Pb/^{238}U$ age for each dated zircon fraction. B. Plot of the weighted average ε_{Hf}(115Ma) vs. the preferred age of each sample. The age of the hydrothermal titanite is shown for comparison. Data are shown in Table 3.

Mala tonalite

In the concordia plot (Fig. 14), the $^{206}Pb/^{238}U$ ages of four data points for zircons from sample AH-130 (Figs. 3, 8K) span the interval from 113.8 ± 0.4 to 116.3 ± 0.4 Ma. Although concordant, the results can also be fitted to a discordia line with a lower intercept at 114.8 ± 0.6 Ma and an upper intercept at 1650 ± 950 Ma. This could be due to the presence of rare recrystallized cores in the zircons (Fig. 13F). However, there is no evidence of such inheritance in the ε_{Hf}(115 Ma) values (Fig. 15, Table 3), which cluster between 7.3 and 7.6, giving a weighted average of 7.4 ± 0.3.

Of the four zircon analyses, the oldest (O40/22 fraction in Table 3) is the least precise, due to a high common lead content and a low $^{206}Pb/^{204}Pb$ ratio of just 158, possibly reflecting the numerous inclusions present in these crystals. Disregarding this analysis, we estimate an age of 114.5 ± 1.0 Ma that encompasses the range and errors of the remaining data points and provides an imprecise but reasonable age for the emplacement of the Mala tonalite.

Hydrothermal titanite

Titanite precipitated during the Main ore stage and not in the postdolerite late-stage calcite sulfides veins (Fig. 9). Its age should therefore unambiguously correspond to the Main ore stage. Two samples of hydrothermal titanite free of ilmenite inclusions were dated. Sample AH-11 is from the Chilena vein in the Raúl mine (Fig. 3) and consists of massive scapolite (with minor prehnite) filling a vein that is cut by K-feldspar-sericite-titanite-sphalerite-galena-chalcopyrite-pyrite veinlets (Fig. 8N). Sample AH-37 was collected at the intersection of the Chilena and Pampa veins, in the Raúl mine (Fig. 3). The sample consists of prehnite, chlorite, pumpellyite, titanite, and chalcopyrite filling a Main ore stage vein brecciated by late calcite (Fig. 8O). The titanite in both samples is interpreted to belong to the Main ore stage and to predate the dolerite dikes and the late-stage calcite sulfides veins (Fig. 9).

Titanite normally contains much more initial common lead than zircon, and this affects the precision of the calculated ages. To evaluate the initial Pb isotope compositions, Pb was analyzed in five samples of pyrite that is interpreted to have precipitated sligthly later than titanite in the paragenetic sequence of the Main ore stage (Table 2, Figs. 9, 12). The weighted average of the Pb isotope compositions of the five pyrite samples, with $^{206}Pb/^{204}Pb$ at 18.606 ± 0.05 percent, $^{207}Pb/^{204}Pb$ at 15.652 ± 0.08 percent, and $^{208}Pb/^{204}Pb$ at 38.577 ± 0.10 percent (Fig. 12), is considered to be a good approximation for the isotope composition of Pb in the hydrothermal fluid. These values are close to those calculated with the Stacey and Kramers (1975) model for average crust (Fig. 12), and the use of either set to correct the initial common lead of titanite gives essentially the same results (<0.1 Ma difference).

Two titanite fractions were dated from sample AH-11 and four fractions from sample AH-37. The analyses indicate moderate (to high) concentrations of U (30–100 ppm) and Th/U (0.14–0.32). The amount of initial common Pb is low in sample AH-37 (0.2–0.3 ppm compared to typical values of 1-3 ppm in titanite; e.g., Corfu and Stone, 1998) but higher in AH-11 titanite (1.2-3.4 ppm), resulting in poor precision for the latter analyses (Table 3). One of the fractions for sample AH-11 (045/S.FC3 in Table 3) gives a younger age than all the other analyzed fractions (Fig. 14), possibly due to lead loss or younger alteration. By contrast, the five other fractions cluster closely and define a concordia age of 115.2 ± 0.3 Ma.

Re-Os Isotopes in Molybdenite

Molybdenite occurs as part of the Main ore stage sequence (Fig. 9). Sample AH-96 is a sample of vein infill consisting of centimeter-sized scapolite (marialite) crystals with interstitial molybdenite and chalcopyrite (Vinchus vein, Raúl mine, level –30, UTM: 32761E, 8595307N). Sample JZ-16 (Pampa vein, Raul mine, level –140, UTM: 327997E, 8594986N) consists of a highly mineralized chalcopyrite-molybdenite vein breccia composed of a mixture of sulfide and actinolized and chloritized wall rock. For each molybdenite sample, polytypes were determined by X-ray diffraction using a 114.6-mm-diameter Gandolfi camera mounted on a Cu anode X-ray source equipped with a Ni filter and working at 40 kV and 30 mA for 3 h.

Sample AH-96 was extremely poor in Re and Os (with ≤0.03 ppm Re and ≤0.3 ppb Os). These concentrations are among the lowest reported for molybdenite and are several orders of magnitude lower than those determined for sample JZ-16 (Table 4) and for molybdenite from other IOCG (e.g., Candelaria, Chile; Mathur et al., 2002) and porphyry copper deposits (e.g., Barra et al., 2003; Berzina et al., 2005). X-ray diffraction showed that this Re-poor molybdenite has a 2H structure. Because of the very low concentrations of Re and Os, the sample was consumed before the proper amount of spikes were determined.

Two runs of sample JZ-16 yielded ages of 121.2 ± 0.5 and 122.8 ± 0.6 Ma, respectively (Table 4). The two ages do not overlap within error (even though the latter includes the uncertainty of the Re decay constant). X-ray diffraction showed that this molybdenite is a mixture of 2H and 3R polytypes.

TABLE 4. Re-Os Isotope Results for Molybdenite from the Raúl-Condestable Deposit

Sample no.	Weight (mg)	Total Re (ppm)	^{187}Re (ppm)	^{187}Os (ppb)	Age (Ma)	Error[1] 2σ (abs)
JZ-16(1)	79.9	332.2	208.8	421.7	121.2	0.5
JZ-16(2)	67.5	422.2	265.4	542.6	122.8	0.6

[1] Includes the error in Re and Os spike calibrations (0.08 and 0.15%, respectively), error in the Re decay constant (0.31%), and analytical error

The two obtained ages might suggest that two or more events of molybdenite deposition occurred. Evidence for this is lacking in sample JZ-16 and is not supported by other samples from the deposit (Fig. 9). Moreover, these ages are inconsistent with the fact that IOCG veins cut the quartz-diorite porphyry, dated at 116.4 ± 0.3 Ma (Table 3, Fig. 16). The

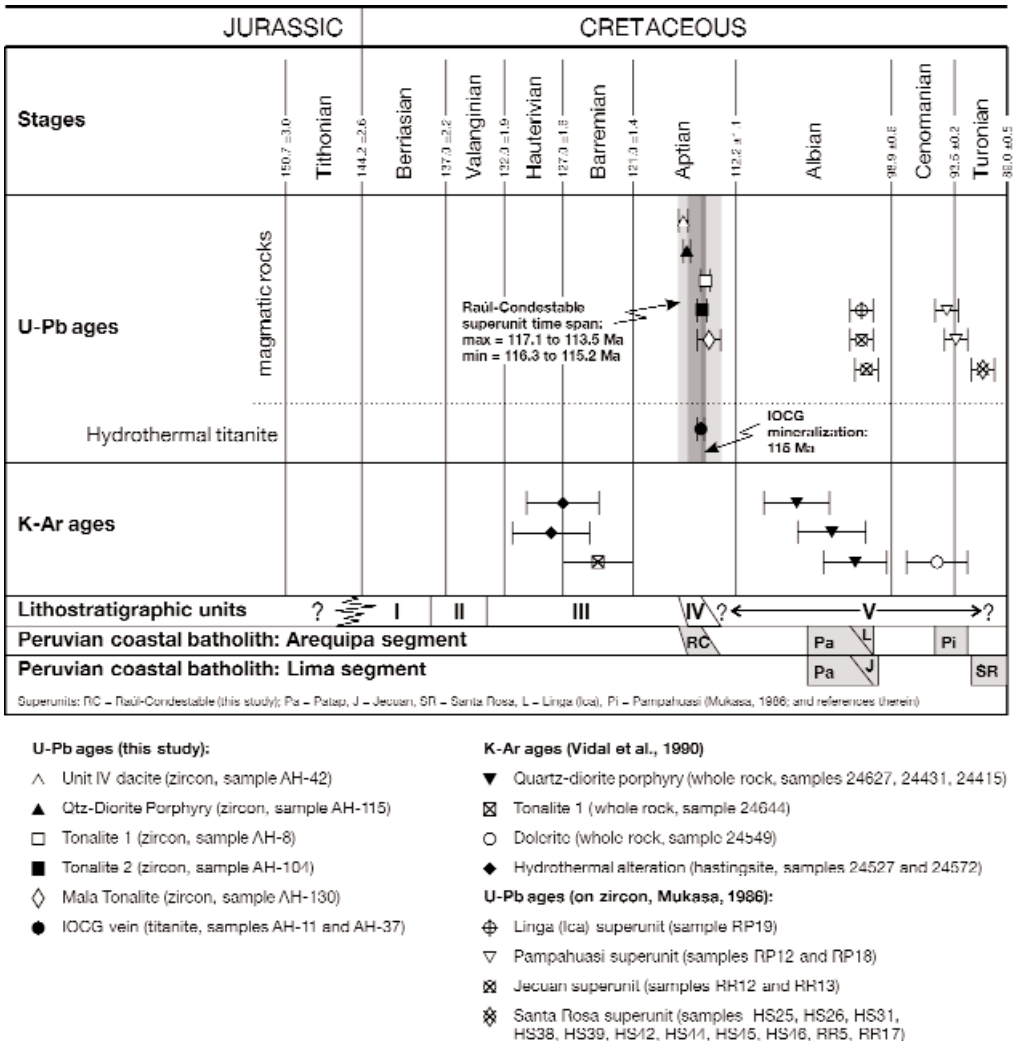

FIG. 16. Summary of isotopic ages of magmatic rocks and hydrothermal minerals from the Raúl-Condestable deposit. Absolute ages of stratigraphic stage boundaries are from Gradstein et al. (1995). Time positions of the first superunits of the Peruvian Coastal batholith are shown for both the Arequipa and Lima segments. Except where radiometric ages are indicated, the age of lithostratigraphic units (see Fig. 5) is based on Salazar and Landa (1993). The U-Pb ages are considered to be reliable; most K-Ar results are not consistent with field relationships (see text, and Mukasa, 1986a). The IOCG mineralization (hydrothermal titanite) is coetaneous within error with the tonalitic intrusions and most probably postdates tonalite 1, at about 115 Ma.

Re-Os ages are therefore doubtful and provide further evidence that the Re-Os system in molybdenite can be sensitive to disturbances (McCandless et al., 1993; Suzuki et al., 2000; Stein et al., 2001; Barra et al., 2003). According to the IOCG paragenetic sequence (Fig. 9), the age of molybdenite is likely closer to 115 Ma (i.e., the age of the dated hydrothermal titanite).

McCandless et al. (1993) argued that Re can only enter the 3R structure, and that Re loss might be related to the transformation from 3R to 2H. It is not presently clear whether there was a partial transformation of an Re-rich 3R polytype to an Re-poor 2H in sample JZ-16 and a total transformation in sample AH-96, or if Re loss occurred without structure transformation. In any case molybdenite from sample JZ-16 has been affected by Re loss, as reflected by the inconsistently old ages obtained and by the age discrepancy between the two measurements. This Re loss could be related to supergene alteration or to post-Main ore stage hydrothermal fluids (e.g., associated with the late minor calcite sulfide veins).

Discussion

The magmatic rocks of the studied district show a volcanic arc geochemical signature, consistent with previous observations by Soler (1991a, b) and with the interpreted shallow-water volcanic island (or coastal) setting of the lithostratigraphic units III and IV (Fig. 5). This is incompatible with the aborted back-arc setting proposed by previous authors (e.g., Cobbing and Pitcher, 1983; Atherton et al., 1985; Atherton and Webb, 1989; Atherton and Aguirre, 1992; Aguirre et al., 1989; Cobbing, 1998). The concentrations of high field strength elements (Nb, Zr, Ti, Y) in pre- and postmineralization basaltic rocks (i.e., early leucogabbro and late Patap Gabbro and dolerite, respectively) could be interpreted to indicate that the basement of the volcanic arc is oceanic crust in this part of the Peruvian coast.

Figure 16 summarizes the U-Pb results presented in this work, together with geochronologic data from the literature. The U-Pb zircon ages between 114.5 ± 1 and 116.4 ± 0.3 Ma obtained from the Raúl-Condestable felsic intrusions (quartz-diorite porphyry, tonalite 1, tonalite 2, and Mala tonalite) are the oldest ages determined for the central coast of Peru, and the unit IV dacite (116.7 ± 0.4 Ma) is the first dated Early Cretaceous volcanic unit in the western Peruvian trough. These ages are 8 to 15 m.y. older than the inferred age of the Patap superunit (Fig. 16; Mukasa, 1986a), which until now was interpreted as the oldest superunit of the Peruvian Coastal batholith (Pitcher, 1985).

We consider that the unit IV volcanic rocks, the quartz-diorite porphyry, and the tonalites of the Raúl-Condestable area belong to the same magmatic suite (i.e., a new Raúl-Condestable superunit), the main characteristics of which are summarized in Table 5. The criteria that were used to define the superunits of the Peruvian Coastal batholith (Atherton and Sanderson, 1985) are fulfilled, as all the igneous rocks assigned to the Raúl-Condestable superunit are closely related in space and time and share common mineralogical and geochemical characteristics. The Mala tonalite was previously attributed to the Jecuan superunit of the Peruvian Coastal batholith (Salazar and Landa, 1993), but the obtained U-Pb zircon age of 114.5 ± 1 Ma is incompatible with the 101.4 ± 1 Ma U-Pb age of this superunit (Mukasa, 1986a). Previously defined superunits of the Coastal batholith did not include extrusive volcanic units, although Moore and Agar (1985) and Pitcher et al. (1985) noted that the emplacement of the batholith at high crustal levels may have been concomitant with magma venting to the surface. In this study, we include the unit IV volcanic rocks in the proposed Raúl-Condestable superunit. The age of the Raúl-Condestable superunit compared to the younger Coastal batholith (~106–37 Ma: Pitcher, 1985; Mukasa, 1986a) is consistent with previous studies that showed an eastward migration of the intrusions through time (e.g., Mukasa, 1986a).

U-Pb zircon ages show that the Raúl-Condestable superunit formed during two magmatic pulses. The first pulse took place at about 116.5 Ma with the emplacement of the base of unit IV (116.7 ± 0.4 Ma) and the quartz-diorite porphyry (116.4 ± 0.3 Ma). The second took place at about 115 Ma and included tonalite 1 (114.8 ± 0.4 Ma) and tonalite 2 (115.1 ± 0.4 Ma), which are coeval with or slightly older than the Mala tonalite (114.5 ± 1 Ma) and tonalite 3 (not dated). Although volcanic equivalents of this second magmatic pulse were not observed, they cannot be excluded and could be expressed in the upper part of unit IV. In this case, unit IV would encompass the whole range of ages obtained on rocks of the Raúl-Condestable superunit (Fig. 16).

Geochemically, these rocks are characterized by a low content of incompatible immobile elements (Nb, Zr, and Y: see

TABLE 5. Characteristics of the Raúl-Condestable Superunit

(intrusive and volcanic rocks of andesitic to dacitic composition)

Rock units		
	Unit IV andesite-dacite	
	Quartz-diorite porphyry	
	Tonalite 1	
	Tonalite 2	
	Tonalite 3	
	Mala Tonalite	
Mineralogy		
Major	Plagioclase (andesite-labrador)	
	Hornblende and/or biotite	
	Quartz	
Accessory	Apatite	
	Magnetite	
	Ilmenite	
	Zircon	
Geochemistry (on a dry basis)		
	SiO_2	58 to 70 wt %
	Nb[1]	7.3 ± 0.8 ppm
	Zr[1]	110.4 ± 4.5 ppm
	Y[1]	7.3 + 0.8/-1.7 ppm
Water content		
High (calcic differentiation trend,[2] amphibole ± biotite fractionation)		
U-Pb zircon ages		116.7 ± 0.4 to 114.5 ± 1 Ma
εHf(115Ma)		5 to 7.5

[1] At 95 percent confidence
[2] Peacock (1931), Sisson and Grove (1993)

Table 1, Fig. 10F) and follow a more calcic trend than the other magmatic rocks of the district. This is illustrated in Figure 11F where the covariance of the CaO and the Na_2O + K_2O contents of least altered samples is plotted against silica (diagram modified from Peacock, 1931). Rocks of the Raúl-Condestable superunit define a broad trend crossing the CaO = Na_2O + K_2O line in the calcic field. In contrast, the unit III lava, the leucogabbro, the unit V lava, and the dolerite, which are older and younger than the Raúl-Condestable superunit, plot on an array in the alkali-calcic field. The Patap Gabbro is more primitive and plots at the intersection of both trends. The calcic trend of the Raúl-Condestable superunit might be indicative of feldspar depression due to high H_2O content (e.g., Sisson and Grove, 1993). This is consistent with the lack of plagioclase fractionation, indicated by the absence of a negative Eu anomaly in the REE data of Injoque (1985) and the absence of anhydrous mafic minerals.

Finally, our U-Pb results confirm crosscutting relationships showing that tonalite 1 and the IOCG-related hydrothermal amphibole (hastingsite) are younger than the quartz-diorite porphyry (Fig. 16). This relationship is inconsistent with previously published K-Ar ages of Vidal et al. (1990) and likely indicates thermal resetting of the K-Ar system in these rocks.

Constraints on the source of the Raúl-Condestable superunit

The lack of old inherited xenocrysts in the various zircon populations analyzed (with one possible exception) suggests a lack of sialic basement in the deposit area, since zircon populations in crustally derived granitic rocks commonly contain large amounts of xenocrystic zircon.

Macfarlane et al. (1990) and Chiaradia and Fontboté (2002) showed that in the central Andes, lead isotope compositions of both ore and igneous rocks are uniform within geographically controlled lead provinces and are apparently much more dependent on the tectonic position than on the timing of extraction. The studied area is part of the lead province Ib (Fig. 1), where no assimilation of old continental basement is observed (Macfarlane et al., 1990). The Pb isotope data on sulfides show higher $^{207}Pb/^{204}Pb$ ratios than normal mantle, indicating a source with mixed mantle and crustal components (e.g., Nazca plate MORB and subducted sediments, respectively; Fig. 12), which Mukasa (1986b), Mukasa et al. (1990), and MacFarlane et al. (1990) suggested corresponds to an enriched upper mantle, but not excluding a minor crustal contribution. Our data agree with this interpretation, since tonalites 1 and 2 fall on a mixing trend between pelagic sediments and Nazca plate MORB values. The fact that Pb of late tonalite 2 has lower $^{207}Pb/^{204}Pb$ ratios than early tonalite 1 might suggest an evolution in the proportions of the source components toward more astenospheric compositions (MORB-like).

Considering that the ε_{Hf}(115Ma) of the depleted mantle (or astenospheric mantle) would have been around 16.8 (calculated with $^{176}Hf/^{177}Hf_{DM(0)}$ = 0.283252, $^{176}Lu/^{177}Hf_{DM(0)}$ = 0.04145, and $^{176}Lu/^{177}Hf_{CRUST(0)}$ = 0.0170; Vervoort and Patchett, 1996), a mixture with a less radiogenic source is necessary to explain the lower ε_{Hf}(115 Ma) values (5.2 ± 0.3–7.5 ± 0.3) obtained on zircons from rocks of the Raúl-Condestable superunit. Possible sources of less radiogenic Hf might include subducted pelagic sediments (Woodhead et al., 2001) or a contribution through partial melting of old continental crust. As noted above, continental crust appears to be absent in the studied region, and it has been postulated that fossil Paleozoic oceanic crust underlies the central coast of Peru. Oceanic crust normally has high ε_{Hf} and alone cannot explain the observed ε_{Hf} values, although a partial contribution cannot be excluded. Therefore, the most likely source is an enriched upper mantle, the Hf isotope composition of which might correspond to a mixture of asthenospheric mantle and subducted pelagic sediments. The ε_{Hf}(115Ma) data show a negative correlation with U-Pb age (Fig. 15), possibly indicating an increasing asthenospheric mantle contribution through time (e.g., Faure, 1986), as suggested for the Pb isotope data of tonalites 1 and 2.

Our results, combined with Hf data obtained on zircons of the Perubar mine area (Fig. 1; $\varepsilon Hf_{(T)}$ between 5.5 and 7.4: Polliand et al., 2005) and of the Domo de Yauli mine district ($\varepsilon Hf_{(T)}$ between –0.9 and +3.1: Beuchat et al., 2003), correlate with Pb isotope data, showing an increase in radiogenic lead from west to east through the Andean Cordillera (Gunnesh et al., 1990; Macfarlane et al., 1990), and are interpreted as corresponding to an increasing contamination of mantle-derived magmas by Precambrian and Paleozoic crust.

The Raúl-Condestable IOCG deposit: A geologic and geochronologic framework

The U-Pb age obtained for the hydrothermal titanite (115.2 ± 0.3 Ma) agrees within errors with the zircon ages of tonalite 1, tonalite 2, and Mala tonalite (114.8 ± 0.4, 115.1 ± 0.4, and 114.5 ± 1 Ma, respectively). The Main ore stage is therefore considered to be coeval with or probably slightly younger than the tonalitic magmatism of the Raúl-Condestable superunit. This is consistent with the fact that the ore feeder veins cut the older unit IV dacite (116.7 ± 0.4 Ma), quartz-diorite porphyry (116.4 ± 0.3 Ma; Fig. 3), and locally tonalite 1, and that the copper ore is associated with a zoned alteration halo surrounding the younger tonalite 1 and 2 intrusions (Figs. 3, 4, 6, 7). Pb isotope compositions of the Main ore stage pyrite and late-stage vein sulfides fall between the whole-rock time-corrected data of tonalite 1 and unit III volcanic rocks and shales (Gunnesh et al., 1990; Fig. 12). Main ore stage sulfides plot closer to the tonalite 1 and late vein sulfides closer to the unit III volcanic rocks. This might indicate that most of the Pb in the Main ore stage was supplied by tonalite 1, with only minor contribution from the enclosing rocks. Tonalite 2 has the least radiogenic Pb values of the area and was apparently not involved as a source of Pb.

The geological, mineralogical, geochemical, and geochronological data presented in this study indicate that the Raúl-Condestable IOCG deposit formed subvolcanically at a depth of 2 to 3 km below the top of unit IV, surrounding a tonalitic stock of the Raúl-Condestable superunit. These findings are incompatible with the volcanic-exhalative model proposed by Ripley and Ohmoto (1977, 1979), Wauschkuhn (1979), and Cardozo (1983), who considered that the magmatism of the Raúl-Condestable superunit took place after ore deposition. This syngenetic interpretation has already been questioned by Atkin et al. (1985), Injoque (1985), and Vidal et al. (1990), who favored ore deposition by replacement. Atkin et al. (1985) and Vidal et al. (1990) compared

Raúl-Condestable to other deposits located within the Peruvian coast (Eliana, Monterrosas, Marcona, and Acari), referring to them as amphibolitic Cu-Fe skarn. However, this kind of Andean Cu-Au deposit is now widely interpreted as belonging to the IOCG class (see Sillitoe, 2003, and references therein).

On an Andean scale, the depth of formation of the Raúl-Condestable deposit, its ore and alteration mineralogy, its age of 115 Ma, and its association with arc magmatism are features similar to the well-documented world-class Candelaria-Punta del Cobre IOCG district in Chile (e.g., Marschik and Fontboté, 2001).

Conclusions

The geology of the Raúl-Condestable area corresponds to a series of superposed volcanic edifices of Early Cretaceous age, which are part of a larger shallow seawater volcanic island or seashore arc. U-Pb zircon ages indicate that felsic magmatic activity took place between 116.7 ± 0.4 and 114.5 ± 1 Ma, defining a new Raúl-Condestable superunit of the Peruvian Coastal batholith. This superunit is located west of the younger main part of the Peruvian Coastal batholith (~106–37 Ma; Pitcher et al., 1985, Mukasa, 1986a) and includes a dacite-andesite lava dome and a subvolcanic quartz-diorite porphyry sill-dike complex emplaced at 116.7 ± 0.4 and 116.4 ± 0.3 Ma, respectively, followed by tonalites intruded between 115.1 ± 0.4 and 114.5 ± 1 Ma. These rocks were products of silica- and water-rich magmas. The intrusive and extrusive nature of this superunit, combined with data from the eastern part of the western Peruvian trough (Polliand et al., 2005), demonstrates that the Peruvian Coastal batholith and the volcano-sedimentary western Peruvian trough are cogenetic parts of the volcanic arc itself, which was active at least in the Aptian (Raúl-Condestable superunit) but may have started already in the Late Jurassic (unit I, or Puente Piedra Group volcanics) and lasted up to the Eocene (e.g., Mukasa, 1986a). This contrasts with previous interpretations which considered the western Peruvian trough (and more specifically the Cañete and Huarmey basins, Fig. 1) and the coastal batholith as being emplaced in an aborted back-arc setting.

In agreement with previous regional studies of the central coast of Peru, the presence of a deep high density (3g/cm3) structure below the studied area, the lack of zircon inheritance in felsic rocks, the flat MORB-normalized HFSE patterns of mafic rocks, and the whole-rock Pb isotope data rule out the presence of Precambrian cratonic basement below the studied area, which possibly lies on a Paleozoic oceanic crust (Haeberlin et al., 2004). Hf isotope data on zircons and whole-rock Pb isotope results are consistent with magmas of the Raúl-Condestable superunit being generated by partial melting of the enriched upper mantle, in agreement with regional Pb-Pb studies cited above.

The Raúl-Condestable IOCG mineralization is directly connected in space and time with the water-rich andesitic (quartz-dioritic) to dacitic (tonalitic) magmatism of the Raúl-Condestable superunit. The mineralization lies in the core of a dacite-andesite volcano, at a paleodepth of 2 to 3 km, surrounding tonalitic intrusions. The U-Pb age of hydrothermal titanite indicates that the mineralization was coeval with (or most probably just followed) the intrusion of the tonalites. Pb isotope data on sulfides and whole rocks suggest that most of the Pb of the IOCG mineralization was supplied by tonalite 1 and not by the less radiogenic late tonalite 2. Finally, the Raúl-Condestable deposit is associated with a zoned alteration that surrounds the tonalitic intrusions, with biotite alteration and quartz stockwork present in the core of the system. This alteration grades laterally to actinolite and upward to sericite and Fe chlorite alteration while the upper periphery is characterized by a hematite-chlorite alteration. Copper is essentially found in association with actinolite alteration.

The geochronologic results of this study confirm that the 110 to 120 Ma age range is a productive time period for Andean IOCG deposits. The characterization of the hydrous intermediate magmatism related to the mineralization, as well as of the subvolcanic position of the deposit and its related alteration pattern, provides further criteria that may be used when exploring for IOCG deposits in a convergent plate tectonic setting.

Acknowledgments

The present investigation was carried out with the support of the Cía. Minera Condestable S.A. and the Swiss National Science Foundation (grant 67836.02). We would like to acknowledge the generous help provided by the Cía. Minera Condestable staff, and in particular: Adalberto Rivadeneira, Patrick Dalla Valle, Marco Carpio, Walter Cruz, and Emilio Cazimirio. Finally, special thanks are due to Robert Busnardo for his kind help in the field of ammonite biostratigraphy. The quality of this manuscript has been substantially improved by the *Economic Geology* reviewers Yves Haeberlin and Ryan Mathur, and their efforts are sincerely acknowledged.

December 22, 2004; April 12, 2006

REFERENCES

Aguirre, L., Levi, B., and Nyström, J.O., 1989, The link between metamorphism, volcanism and geotectonic setting during the evolution of the Andes: Geological Society Special Publication 43, p. 223–232.

Atkin, B.P., Injoque, J., and Harvey, P.K., 1985, Cu-Fe amphibole mineralization in the Arequipa segment, *in* Pitcher, W.S., Atherton, M.P., Cobbing, E.J., and Beckingsale, R.D., eds., Magmatism at the plate edge: The Peruvian Andes: Glasgow, UK, Blackie, p. 261–270.

Atherton, M.P., and Aguirre, L., 1992, Thermal and geotectonic setting of Cretaceous volcanic rocks near Ica, Peru, in relation to Andean crustal thinning: Journal of South American Earth Sciences, v. 5, p. 47–69.

Atherton, M.P., and Sanderson, L.M., 1985, The chemical variation and evolution of the super-units of the segmented Coastal batholith, *in* Pitcher, W.S., Atherton, M.P., Cobbing, E.J., and Beckingsale, R.D., eds., Magmatism at the plate edge: The Peruvian Andes: Glasgow, UK, Blackie, p. 208–227.

Atherton, M.P., and Webb, S., 1989, Volcanic facies, structure, and geochemistry of the marginal basin rocks of central Peru: Journal of South American Earth Sciences, v. 2, p.241–261.

Atherton, M.P., Warden, V., and Sanderson, L.M., 1985, The Mesozoic marginal basin of Central Peru: A geochemical study of within-plate-edge volcanism. *in* Pitcher, W.S., Atherton, M.P., Cobbing, E.J., and Beckingsale, R.D., eds., Magmatism at the plate edge: The Peruvian Andes: Glasgow, UK, Blackie, p. 47–58.

Barra, F., Ruiz, J., Mathur, R., and Titley, S., 2003, A Re-Os study of sulfide minerals from the Bagdad porphyry Cu-Mo deposit, northern Arizona, USA: Mineralium Deposita, v. 38, p. 585–596.

Beckinsale, R.D., Sanchez-Fernandez, A.W., Brook, M., Cobbing, E.J., Taylor, W.P., and Moore, N.D., 1985, Rb-Sr whole-rock isochron and K-Ar age determinations for the Coastal batholith of Peru, *in* Pitcher, W.S., Atherton, M.P., Cobbing, E.J., and Beckingsale, R.D., eds., Magmatism at the plate edge: The Peruvian Andes: Glasgow, UK, Blackie, p. 177–202.

Benavides-Cáceres, V., 1999, Orogenic evolution of the Peruvian Andes: The Andean cycle: Society of Economic Geologists Special Publication 7, p.61–107.

Berzina, A.N., Sotnikov, V.I., Economou-Eliopoulos, M., and Eliopoulos, D.G., 2005, Distribution of rhenium in molybdenite from porphyry Cu-Mo and Mo-Cu deposits of Russia (Siberia) and Mongolia: Ore Geology Reviews, v. 26, p. 91–113.

Beuchat, S., Schaltegger, U., Moritz, R., Chiaradia, M., Cosca, M., and Fontignie, D., 2003, Resolving Miocene magmatic and mineralizing events in the Zn-Pb-Ag-Cu Domo de Yauli district (Peru) by high-precision geochronology, *in* Beuchat, S., Geochronological, structural, isotopes and fluid inclusion constrains of the polymetallic Domo de Yauli district, Peru: Ph.D. thesis, Geneva, Switzerland, University of Geneva, Terre et Environnement, v. 41, 130 p.

Blichert-Toft, J., and Albarède, F., 1997, The Lu-Hf isotope geochemistry of chondrites and the evolution of the mantle-crust system: Earth Planetary Science Letters, v. 148, p.243–258.

Cardozo, M., 1983, Raúl als Beispiel vulkanogener Kupferlagerstätten im Copará-Metallotekt, Zentralperu: Unpublished Ph.D. thesis, Heidelberg, Ruprecht-Karls Universität, 240 p.

Chiaradia, M., and Fontboté, L., 2002, Lead isotope systematics of Late Cretaceous-Tertiary Andean arc magmas and associated ores between 8°N and 40°S: Evidence for latitudinal mantle heterogeneity beneath the Andes: Terra Nova, v. 14, p. 337–342.

Chiaradia, M., Fontboté, L., and Paladines, A., 2004, Metal sources in mineral deposits and crustal rocks of Ecuador (1°N-4°S): a lead isotope synthesis: Economic Geology, v. 99, p. 1085–1106.

Cobbing, E.J., 1978, The Andean geosyncline in Peru, and its distinction from Alpine geosynclines: Journal of the Geological Society [London], v. 135, p. 207–218

——1985, The tectonic setting of the Peruvian Andes, *in* Pitcher, W.S., Atherton, M.P., Cobbing, E.J., and Beckingsale, R.D., eds., Magmatism at the plate edge: The Peruvian Andes, Glasgow, UK, Blackie, p. 3–12.

——1998, The Coastal batholith and other aspects of Andean magmatism in Peru: Boletín de la Sociedad Geológica del Perú, v. 88, p. 5–20.

Cobbing, E.J., and Pitcher, W.S., 1983, Andean plutonism in Peru and its relationship to volcanism and metallogenesis at a segmented plate edge: Geological Society of America Memoir, v. 159, p. 277–291.

Corfu, F., 2004, U-Pb age, setting, and tectonic significance of the anorthosite-mangerite-charnockite-granite-suite, Lofoten-Vesterålen, Norway: Journal of Petrology, v. 45, p. 1799–1819.

Corfu, F., and Andersen, T.B., 2002, U-Pb ages of the Dalsfjord Complex, SW-Norway, and their bearing on the correlation of allochtonous crystalline segments of the Scandinavian Caledonides: International Journal of Earth Sciences, v. 91, p. 955–963.

Corfu, F., and Stone, D., 1998, The significance of titanite and apatite U-Pb ages: Constraints for the post-magmatic thermal-hydrothermal evolution of a batholithic complex, Berens River area, northwestern Superior province: Geochimica et Cosmochimica Acta, v. 62, p. 2979–2995.

Corfu, F., Hanchar, J.M., Hoskin, P.W.O., and Kinny, P., 2003, Atlas of zircon textures: Reviews in Mineralogy and Geochemistry, v. 53, p. 469–500.

Couch, R., Whitsett, R., Huehn, B., and Briceno-Guarupe, L., 1981, Structure of the continental margin of Peru and Chile: Geological Society of America Bulletin, v. 154, p. 703–726.

de Haller, A., 2000, The Raul-Condestable iron oxides-Cu-Au deposit, Lima department, Peru: Preliminary results: Luleå University of Technology Research Report 2000:6, p. 8–11.

——2006, The Raúl-Condestable iron oxide copper-gold deposit, central coast of Peru: Ph.D. thesis, Geneva, Switzerland, University of Geneva, Terre et Environnement, v. 58, 123 p.

de Haller, A., Zúñiga, A. J., and Fontboté, L., 2001, Geology of the Raul-Condestable iron oxide-copper-gold deposit, central coast of Peru [abs.]: Geological Society of America Program with Abstracts, v. 33, p. A129.

de Haller, A., Zúñiga, A. J., Corfu, F., and Fontboté, L., 2002, The iron oxide-Cu-Au deposit of Raúl-Condestable, Mala, Lima, Peru [abs.]: Congreso Geológico Peruano, 11th, Resúmenes, p. 80.

Faure, G., 1986, Principles of isotope geology, 2nd ed.: New York, Wiley, 589 p.

Gradstein, F.M., Agterberg, F.P., Ogg, J.G., Hardenbol, J., Van Veen, P., Thierry, J., and Huang, Z., 1995, A Triassic, Jurassic and Cretaceous time scale, geochronology time scales and global stratigraphic correlation: Society for Sedimentary Geology (SEPM) Special Publication 54, p. 95–126.

Guevara, C., 1980, Él Grupo Casma del Perú central entre Trujillo y Mala: Boletín de la Sociedad Geológica del Perú, v. 67, p. 73–83.

Gunnesch, K.A., Baumann, A., and Gunnesch, M., 1990, Lead isotope variations across the Central Peruvian Andes: Economic Geology, v. 85, p. 1384–1401

Haeberlin, Y., Moritz, R., Fontboté, L., and Cosca, M., 2004, Carboniferous orogenic gold deposits at Pataz, Eastern Andean Cordillera, Peru: Geological and structural framework, paragenesis, alteration, and $^{40}Ar/^{39}Ar$ geochronology: Economic Geology, v. 99, p. 73–112.

Haederle M., and Atherton M.P., 2002, Shape and intrusion style of the Coastal batholith, Peru: Tectonophysics, v. 345, p. 17–28.

Hoskin, P.W.O., and Schaltegger, U., 2003, The composition of zircon and igneous and metamorphic petrogenesis: Reviews in Mineralogy and Geochemistry, v. 53, p. 27–62.

Injoque, J., 1985, Geochemistry of the Cu-Fe-amphibole skarn deposits of the Peruvian central coast: Unpublished Ph.D. thesis, UK, University of Nottingham, 359 p.

——2002, Fe oxide-Cu-Au deposits in Peru: An integrated view, *in* Porter, T.M., ed., Hydrothermal iron oxide copper-gold and related deposits: A global perspective, vol. 2: Adelaide, Porter GeoConsultancy Publishing, p. 97–113.

Jaillard, E., Soler, P., Carlier, G., and Mourier, T., 1990, Geodynamic evolution of the northern and central Andes during early to middle Mesozoic times: A Thetyan model: Journal of the Geological Society of London, v. 147, p. 1009–1022.

Jones, P.R., 1981, Crustal structures of the Peru continental margin and adjacent Nazca plate, 9°S latitude: Geological Society of America Memoir 154, p. 423–444.

Krogh, T.E., 1982, Improved accuracy of U-Pb zircon ages by the creation of more concordant systems using an air abrasion technique: Geochimica et Cosmochimica Acta, v. 46, p. 637–649.

Le Bas, M.J., Le Maître, R.W., Streckeisen, A., and Zanettin, B., 1986, A chemical classification of volcanic rocks based on the total alkali-silica diagram: Journal of Petrology, v. 27, p. 745–750.

Ludwig, K.R., 1999, Isoplot/Ex version 2.03: A geochronological toolkit for Microsoft Excel: Berkeley Geochronology Center Special Publication, v. 1, p. 1–43.

Macfarlane, A.W., Marcet, P., LeHuray, A.P., and Petersen, U., 1990, Lead isotope provinces of the Central Andes inferred from ores and crustal rocks: Economic Geology, v. 85, p. 1857–1880.

Marschik, R., and Fontboté, L., 2001, The Candelaria-Punta del Cobre iron oxide Cu-Au (-Zn-Ag) deposits, Chile: Economic Geology, v. 96, p. 1799–1826.

Mathur R., Marschik R., Ruiz J., Munizaga F., Leveille R.A., and Martin W., 2002, Age of mineralization of the Candelaria Fe oxide Cu-Au deposit and the origin of the Chilean iron belt, based on Re-Os isotopes: Economic Geology, v. 97, p. 59–71.

McCandless, T.E., Ruiz, J., and Campbell, A.R., 1993, Rhenium behavior in molybdenite in hypogene and near-surface environments: Implications for Re-Os geochronometry: Geochimica et Cosmochimica Acta, v. 57, p. 889–905.

Meschede, M., 1986, A method of discriminating between different types of mid-ocean ridge basalts and continental tholeiites with the Nb-Zr-Y diagram: Chemical Geology, v. 56, p. 207–218.

Moore, N.D., and Agar, R.A., 1985, Variations along a batholith: the Arequipa segment of the Coastal batholith of Peru, *in* Pitcher, W.S., Atherton, M.P., Cobbing, E.J., and Beckingsale, R.D., eds., Magmatism at the plate edge: The Peruvian Andes: Glasgow, UK, Blackie, p. 108–118

Mukasa, S.B., 1986a, Zircon U-Pb ages of super-units in the Coastal batholith, Peru: Implications for magmatic and tectonic processes: Geological Society of America Bulletin, v. 97, 241–254.

——1986b, Common Pb isotope compositions of the Lima, Arequipa and Toquepala segments in the Coastal batholith, Peru: Implications for magmatogenesis: Geochimica et Cosmochimica Acta, v. 50, p. 771–782.

Mukasa, S.B., and Tilton, G.R., 1985a, Zircon U-Pb ages of super-units in the Coastal batholith, Peru, *in* Pitcher, W.S., Atherton, M.P., Cobbing, E.J., and Beckingsale, R.D., eds., Magmatism at the plate edge: The Peruvian Andes: Glasgow, UK, Blackie, p. 203–207.

——1985b, Pb isotope systematics as a guide to crustal involvement in the generation of the Coastal batholith, Peru, *in* Pitcher, W.S., Atherton, M.P., Cobbing, E.J., and Beckingsale, R.D., eds., Magmatism at the plate edge: The Peruvian Andes: Glasgow, UK, Blackie, p. 235–238.

Mukasa, S.B., Vidal C., C.E., and Injoque-Espinoza, J., 1990, Pb isotope bearing on the metallogenesis of sulfide ore deposits in Central and Southern Peru: Economic Geology, v. 85, p. 1438–1446.

Myers, J.S., 1974, Cretaceous stratigraphy and structure, Western Andes of Peru between latitudes 10°-10°30': American Association of Petroleum Geologists Bulletin, v. 58, p. 474–487.

Noble, D.C., Vidal, C.E., Angeles Z., C., Wise, J.M., Zanetti, K.A., Spell, T.L., in press (a), Caldera-related ash-flow tuff of Paleocene age in central Peru and its significance for Late Cretaceous and Paleocene magmatism, sedimentation and tectonism, *in* Arce Helberg, J.E., ed., Volumen Especial N°6 Alberto Giesecke Matto: Sociedad Geologica del Perú.

Noble, D.C., Ríos C., A, Vidal, C.E., Spell, T.L., Zanetti, K.A., Angeles Z., C., Ochoa A., J.L., Cruz C., S.R., in press (b), Late Cretaceous basalt in the Río Mala valley, central Peru: Evidence for extention and mafic magmatism prior to Late Cretaceous-Paleocene plutonism and silicic volcanism, *in* Arce Helberg, J.E., ed., Volumen Especial N°6 Alberto Giesecke Matto: Sociedad Geologica del Perú,

Osterman, G., Cardozo, M., and Wauschkuhn, A., 1983, Descripción y correlación de los depósitos volcánicos-sedimentarios del Cretásico Inferior en la región Lima-Cañete: Boletín de la Sociedad Geológica del Perú, v. 70, p. 35–46.

Palacios, O., Caldas, J., and Vela, C., 1992, Geología de los cuadrángulos de Lima, Lurín, Chancay y Chosica: Instituto Geológico Minero y Metalúrgico del Perú, Lima, Peru, Boletín 43, Serie A: Carta Geológica Nacional, 163 p.

Peacock, M.A., 1931, Classification of igneous rock series: Journal of Geology, v. 39, p. 54–67.

Pearce, J.A., 1983, Role of the sub-continental lithosphere in magma genesis at active continental margins, *in* Hawkesworth, C.J., and Norry, M.J., eds., Continental basalts and mantle xenoliths: Nantwich, Shiva, p. 230–249.

Pearce, J.A., and Cann, J.R., 1973, Tectonic setting of basic volcanic rocks determined using trace element analyses: Earth and Planetary Science Letters, v. 19, p. 290–300.

Pearce, J.A., and Norry, M.J., 1979, Petrogenetic implications of Ti, Zr, Y, and Nb variations in volcanic rocks: Contributions to Mineralogy and Petrology, v. 69, p. 33–47.

Pearce, J.A., Harris, N.B.W., and Tindle, A.G., 1984, Trace element discrimination diagrams for the tectonic interpretation of granitic rocks: Journal of Petrology, v. 25, p. 956–983.

Pfeifer, H.R., Lavanchy, J.C., and Serneels, V., 1991, Bulk chemical analysis of geological and industrial materials by X-Ray fluorescence, recent developments and application to materials rich in iron oxide: Journal of Trace Microprobe Techniques, v. 9, p. 127–147.

Pitcher, W.S., 1985, A multiple and composite batholith, *in* Pitcher, W.S., Atherton, M.P., Cobbing, E.J., and Beckingsale, R.D., eds., Magmatism at the plate edge: The Peruvian Andes: Glasgow, UK, Blackie, p. 93–101.

Pitcher, W.S., Atherton, M.P., Cobbing, E.J., and Beckinsale, R.D., 1985, A model for the Coastal batholith, *in* Pitcher, W.S., Atherton, M.P., Cobbing, E.J., and Beckingsale, R.D., eds., Magmatism at the plate edge: The Peruvian Andes: Glasgow, UK, Blackie, p. 239–240.

Polliand, M., Schaltegger, U., Frank, M., and Fontboté, L., 2005, Formation of intra-arc volcano-sedimentary basins in the western flank of the central Peruvian Andes during Late Cretaceous oblique subduction—field evidence and constraints from U-Pb ages and Hf isotopes: International Journal of Earth Sciences, v. 94, p. 231–242.

Pupin, J.P., 1980, Zircon and granite petrology: Contributions to Mineralogy and Petrology, v. 73, p. 207–220.

Regan, P.F., 1985, The early basic intrusions, *in* Pitcher, W.S., Atherton, M.P., Cobbing, E.J., and Beckingsale, R.D., eds., Magmatism at the plate edge: The Peruvian Andes: Glasgow, UK, Blackie, p. 72–90.

Rios, C., 2000, El genero Olcostephanus en el Valanginiano Peruano y Americano: fosiles presentes en la mina Raúl-Condestable [abs.]: X Congreso Peruano de Geología, Lima, Volumen de Resúmenes, Sociedad Geológica del Perú, Publicación Especial N°2, p. 230.

Ripley, E.M., and Ohmoto, H., 1977, Mineralogic, sulfur isotope, and fluid inclusion studies of the strata-bound copper deposits at the Raul mine, Peru: Economic Geology, v. 72, p. 1017–1041.

——1979, Oxygen and hydrogen isotopic studies of ore deposition and metamorphism at the Raul mine, Peru: Geochimica et Cosmochimica Acta, v. 43, p. 1633–1643.

Rivera, R., Petersen, G., and Rivera, M., 1975, Estratigrafía de la costa de Lima: Boletín de la Sociedad Geológica del Perú, v. 45, p. 159–186.

Salazar, H., and Landa, C., 1993, Geología de los cuadrángulos de Mala, Lunahuaná, Tupe, Conayca, Chincha, Tantará y Castrovirreyna: Instituto Geológico Minero y Metalúrgico del Perú, Lima, Peru, Boletín 44, Serie A: Carta Geológica Nacional, 91 p.

Scott, R.W., and Aleman, A., 1984, Stylina Columbaris n. sp. in an Early Cretaceous coral biostrome, Peru: Journal of Paleontology, v. 58, p. 1136–1142.

Schaltegger, U., Zeilinger, G., Frank, M., and Brug, J.-P., 2002, Multiple mantle sources during island arc magmatism: U-Pb and Hf isotopic evidence from the Kohistan arc complex, Pakistan: Terra Nova, v. 14, p. 461–468.

Selby, D., and Creaser, R.A., 2004, Macroscale NTIMS and microscale LA-MC-ICP-MS Re-Os isotopic analysis of molybdenite: Testing spatial restrictions for reliable Re-Os age determinations, and implications for the decoupling of Re and Os within molybdenite: Geochimica et Cosmochimica Acta, v. 68, p. 3897–3908.

Sillitoe, R.H., 2003, Iron oxide-copper-gold deposits: an Andean view: Mineralium Deposita, v. 38, p. 787–812.

Silver, L.T., and Deutsch, S., 1963, Uranium-lead isotopic variations in zircons: A case study: Journal of Geology, v. 71, p. 721–758.

Sisson, T.W., and Grove, T.L., 1993, Experimental investigation of the role of H_2O in calc-alkaline differentiation and subduction zone magmatism: Contributions to Mineralogy and Petrology, v. 113, p. 143–166.

Soler, P., 1991a, Contribution à l'étude du magmatisme associé aux marges actives—petrographie, géochimie et géochimisme isotopique du magmatisme Crétacé à Pliocène le long d'une transversale des Andes du Pérou central—implications géodynamiques et métallogéniques: Unpublished Thèse de doctorat d'Etat, France, Université Pierre et Marie Curie, Paris VI, 846 p.

——1991b, El volcanismo Casma del Perú Central: cuenca marginal abortada o simple arco volcanico?: VII Congreso Peruano de Geología, Lima, Volumen de Resúmenes Extendidos, Sociedad Geológica de Perú, p. 659–663.

Stacey, J.S., and Kramers, J.D., 1975, Approximation of terrestrial lead isotope evolution by a two stage model: Earth and Planetary Science Letters, v. 26, p. 207–221

Stein, H.J., Markey, R.J., Morgan, J.W., Hannah, J.L., and Schersten, A., 2001, The remarkable Re-Os chronometer in molybdenite: How and why it works: Terra Nova, v. 13, p. 479–486.

Suzuki, K., Kagi, H., Nara, M., Takano, B., and Nozaki, Y., 2000, Experimental alteration of molybdenite: Evaluation of the Re-Os system, infrared spectroscopic profile and polytype: Geochimica et Cosmochimica Acta, v. 64, p. 223–232.

Vela, C., 1997, Nueva concepción estratigráfica de la subcuenca de Lima [ext. abs.]: IX Congreso Peruano de Geología, Resúmenes Extendidos, Sociedad Geológica de Perú, Vol. Esp. 1, Lima, p. 409–412.

Vervoort, J.D., and Patchett, P.J., 1996, Behaviour of hafnium and neodymium isotopes in the crust: Constraints from Precambrian crustally derived granites: Geochimica Cosmochimica Acta, v. 60, p. 3717–3733.

Vidal, C., Injoque, J., Sidder, G. B., and Mukasa, S. B., 1990, Amphibolitic Cu-Fe skarn deposits in the Central Coast of Peru: Economic Geology, v. 85, p. 1447–1461.

Wasteneys, H.A., Clark, A.H., Farrar, E., and Langridge, R.J., 1995, Grenvillian granulite-facies metamorphism in the Arequipa Massif: A Laurentia-Gondwana link: Earth and Planetary Science Letters, v. 132, p. 63–73.

Wauschkuhn, A., 1979, Geology, mineralogy and geochemistry of the stratabound Cu deposits in the Mesozoic Coastal belt of Peru: Boletín de la Sociedad Geológica del Perú, v. 62, p. 161–192.

Williams, P.J., Barton, M.D., Johnson, D.A., Fontboté, L., de Haller, A., Mark, G., Oliver, N.H.S., and Marschik, R., 2005, Iron oxide copper-gold deposits: Geology, space-time distribution, and possible modes of origin: Economic Geology 100th Anniversary Volume, p. 371–405.

Wilson, D.V., 1985, The deeper structure of the Central Andes and some geophysical constraints, *in* Pitcher, W.S., Atherton, M.P., Cobbing, E.J., and Beckingsale, R.D., eds., Magmatism at the plate edge: The Peruvian Andes: Glasgow, UK, Blackie, p. 13–18.

Wilson, J.J., 1963, Cretaceous stratigraphy of central Andes of Peru: Bulletin of the American Association of Petroleum Geologists, v. 47, p. 1–34.

Winchester, J.A., and Floyd, P.A., 1977, Geochemical discrimination of different magma series and their differentiation products using immobile elements: Chemical Geology, v. 20, p. 325–343.

Woodhead, J.D., Hergt, J.M., Davidson, J.P., and Eggins, S.M., 2001, Hafnium isotope evidence for "conservative" element mobility during subduction zone processes: Earth and Planetary Science Letters, v. 192, p. 331–346.

Wright, C.W., Callomon, J.H., and Howarth, M.K., 1996, Treatise on Invertebrate Paleontology, part L Mollusca 4, Volume 4, Cretaceous Ammonoidea: Geological Society of America and University of Kansas, rev. ed., XX + 362 p.